

AD-A101 681

BELL AEROSPACE TEXTRON NEW ORLEANS LA  
COLD WATER PIPE (CWP) MODEL FEASIBILITY TEST. (U)  
FEB 79 V GRIFFITH, J RYKEN, W DUKES

F/6 13/11

N00014-78-C-0759

NL

UNCLASSIFIED

2531-928002

1 of 1  
409681

END  
DATE  
FILED  
8-8-81  
DTIC

AD A101681

LEVEL  
①

NEW ORLEANS OPERATIONS  
**Bell Aerospace TEXTRON**  
Division of Textron Inc

COLD WATER PIPE (CWP)

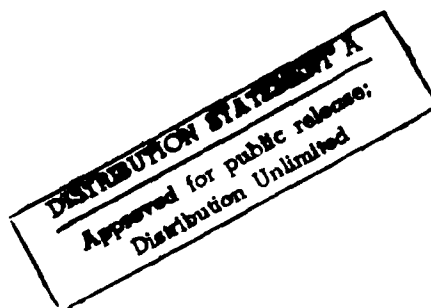
MODEL FEASIBILITY TEST FINAL REPORT

CONTRACT N00014-78-C-0759 *Ric*

Report 2531-928002

FEBRUARY, 1979

Prepared For  
Naval Ocean Research and Development Activity  
Naval Oceanographic Laboratory  
Ocean Technology Division



Prepared by V. Griffith  
J. Ryken  
W. Dukes

*R. Decrevel*  
R. Decrevel  
Project Manager

FILE COPY

3/24/81 81721031

## TABLE OF CONTENTS

	<u>Page</u>
List of Illustrations	iii
List of Tables	vi
Nomenclature	vii
1. INTRODUCTION	1
2. OBJECTIVES	2
3. SCALING STUDY	3
3.1 Model Pipe Geometry	3
3.2 Reynolds Number Scaling	3
3.3 Froude Scaling	5
3.4 Current-Velocity Scaling	6
3.5 Ballast-Weight Scaling	10
3.6 Model Material Stiffness	10
3.7 Application of Model Results to Full Scale	13
4. MODEL DESCRIPTION	14
5. FACILITY AND INSTRUMENTATION	24
6. RANGE OF TESTS	26
7. DATA REDUCTION	28
7.1 Lateral Displacement Computation	33
8. RESULTS	34
8.1 Static Ring Buckling Tests	34
8.2 Vibration Tests	34
8.3 Tow Tests	47
9. INTERPRETATION OF RESULTS	64
9.1 Static Ring Buckling Tests	64
9.2 Vibration Tests	65
9.2.1 Vibration Amplitudes	65
9.2.2 Ballast Effects	66
9.2.3 Effective Water Mass	66

Accession for  
NTIS GEN&I  
DTIC TAB  
Unannounced  
Justification  
By \_\_\_\_\_  
Distribution/  
Availability Class  
Approved by \_\_\_\_\_  
Dist Special  
  
A

2531-928002

TABLE OF CONTENTS (Cont)

	<u>Page</u>
9.2.4 Pressure Effects	66
9.2.5 Vibration Modes	67
9.2.6 Extrapolation to Full Scale	67
9.3 Tow Tests	69
9.3.1 First-Mode Vibration	69
9.3.2 Higher Modes	70
9.3.3 Frequency and Drag Relations	70
9.3.4 Higher-Mode Test Methods	71
9.3.5 Extrapolation to Full Scale	72
9.3.6 Local Oscillations	72
10. CONCLUSIONS AND RECOMMENDATIONS	74
10.1 Conclusions	74
10.2 Recommendations	74
REFERENCES	76

LIST OF ILLUSTRATIONS

<u>Figure</u>		<u>Page</u>
1	COLD WATER PIPE MODEL - ATTAINABLE REYNOLDS NUMBER RANGE	5
2	TYPICAL 30-FOOT-INSIDE-DIAMETER FLEXIBLE CWP	7
3	LENGTHS OF PIPE WHERE VORTEX FREQUENCIES MATCH STRING MODE FREQUENCIES	11
4	GEOMETRY OF MODEL	15
5	CWP MODEL COMPONENTS	16
6	INSIDE VIEW OF CWP MODEL	17
7	SCHEMATIC OF FLEXIBLE CWP MODEL IN TOW TANK	18
8	ASSEMBLED CWP MODEL DURING AIR-INFLATION CHECK	19
9	SCHEMATIC OF PULSED JET SYSTEM FOR VIBRATION TESTS	20
10	PULSED WATERJET SYSTEM	21
11	GENERAL VIEW OF TOW CARRIAGE	25
12	MODEL UNDER TEST	25
13	ACCELEROMETER CALIBRATION	29
14	PENDULUM MODE AMPLITUDE CORRECTION FACTORS	31
15	TYPICAL OSCILLOGRAPH RECORD: RUN 9-5	32
16	VARIATION OF ANNULUS PRESSURE WITH REDUCED CORE PRESSURE (BALLAST WEIGHT, 13 LB)	35
17	VARIATION OF ANNULUS PRESSURE WITH REDUCED CORE PRESSURE (BALLAST WEIGHT, 36.05 LB)	36
18	APPROXIMATE GEOMETRY OF COLLAPSED PIPE	37
19	VARIATION OF PIPE OSCILLATION WITH FORCING FREQUENCY, RUN 11 (BALLAST WEIGHT, 13 LB)	38

## LIST OF ILLUSTRATIONS (Cont)

<u>Figure</u>		<u>Page</u>
20	VARIATION OF PIPE OSCILLATION WITH FORCING FREQUENCY, RUNS 8, 9, AND 10 (BALLAST WEIGHT, 36.05 LB)	39
21	VARIATION OF PIPE OSCILLATION WITH FORCING FREQUENCY, RUNS 14 AND 15 (BALLAST WEIGHT, 83 LB)	40
22	VARIATION OF NATURAL FREQUENCY WITH BALLAST	41
23	VIBRATION TEST PEAK RESPONSE AMPLITUDE VERSUS PEAK RESPONSE FREQUENCY	44
24	DECAYING OSCILLATION: RUN 11-10	46
25	VARIATION OF PIPE LATERAL DISPLACEMENT AND FREQUENCY WITH SPEED, RUN 16 (BALLAST WEIGHT, 13 LB)	48
26	VARIATION OF PIPE LATERAL DISPLACEMENT AND FREQUENCY WITH SPEED, RUN 17 (BALLAST WEIGHT, 13 LB)	49
27	VARIATION OF PIPE LATERAL DISPLACEMENT AND FREQUENCY WITH SPEED, RUN 19 (BALLAST WEIGHT, 36 LB)	50
28	VARIATION OF PIPE LATERAL DISPLACEMENT AND FREQUENCY WITH SPEED, RUN 20 (BALLAST WEIGHT, 83 LB)	51
29	VARIATION OF PIPE LATERAL DISPLACEMENT AND FREQUENCY WITH SPEED, RUN 21 (BALLAST WEIGHT, 83 LB)	52
30	FREQUENCY OF PEAK RESPONSE VERSUS BALLAST WEIGHT DURING TOW TESTS	53
31	TOW TEST PEAK RESPONSE AMPLITUDE VERSUS PEAK RESPONSE FREQUENCY	54
32	AMPLITUDE VARIATIONS DURING CONSTANT VELOCITY TOW	56
33	HIGH-FREQUENCY OSCILLATIONS, RUN 21-3, TOW VELOCITY = 0.805 FT/SEC	57
34	HIGH-FREQUENCY OSCILLATIONS AT EXPANDED TIME SCALE, RUN 19-8, TOW VELOCITY = 1.1 FT/SEC	58

LIST OF ILLUSTRATIONS (Cont)

<u>Figure</u>		<u>Page</u>
35	EXAMPLE OF PENDULUM-MODE SHAPE, TOW RUN 21-4, $f = 0.172$ Hz	60
36	VARIATION OF PIPE DEFLECTION (AFT) WITH SPEED	61
37	PHOTOGRAPH OF FLOW PATTERN AROUND MODEL CWP	62
38	LOCATION OF SPOILERS	63
39	SKETCH OF OBSERVED SECOND-MODE SHAPE	68

LIST OF TABLES

<u>Table</u>		<u>Page</u>
I	EXAMPLE OF MODEL SCALING	6
II	SCALING TO REPRESENTATIVE 30-FOOT-ID CWP	8
III	SCALING TO REPRESENTATIVE 6-FOOT-ID CWP	9
IV	MODEL PARTICULARS	22
V	SIGNIFICANT MATERIAL PARTICULARS	23
VI	SUMMARY OF TESTS	26
VII	COMPARISON OF DATA FROM UPPER, MIDDLE, AND LOWER ACCELEROMETERS	42

### NOMENCLATURE

$a_n$	Constants in beam frequency equation
$C_d$	Drag coefficient
$C$	Logarithmic decrement
$D$	Diameter (ft)
$e$	Base for natural logarithms (2.718)
$E$	Material tensile stiffness $\left( \frac{1b}{in^2} : \frac{in.}{in.} \right)$
$EA$	Axial stiffness (lb/in/in)
$EI$	Bending stiffness (lb-in <sup>2</sup> )
$f$	Frequency of oscillation (Hz)
$f_n$	Frequency (Hz)
$f_p$	Frequency, pendulum mode
$f_s$	Frequency, string mode
$f_v$	Frequency, vortex
$g$	Acceleration of gravity (32.2 ft/sec <sup>2</sup> )
$I$	Moment of inertia of pipe, water, and ballast about pivot point
$K$	Calibration factor (1.2 deg/square)
$x$	Distance from the apparent pivot point to the accelerometer
$L$	Length of pipe plus ballast can (10.25 ft)
$L/D$	Length-to-diameter ratio
$L_P$	Length from pivot to cg of ballast weight
$n$	Mode number
$N$	Accelerometer output (g)
$OD$	Outside diameter of the pipe (0.75 ft)

P	Pressure (psi)
PA	Annulus pressure (inches of water)
PC	Core pressure (inches of water)
R	Bottom accelerometer reading (peak to peak) squares on record
RN	Reynolds number
R/R <sub>critical</sub>	Damping ratio
S	Lateral deflections (ft)
SN	Strouhal number
t	Time (sec)
T	Tension
u	Mass/unit length
v	Velocity (ft/sec)
w	Weight (lb)
w <sub>b</sub>	Ballast weight (in water)
w <sub>B</sub>	Ballast weight corrected for buoyancy
ÿ	Acceleration (ft/sec <sup>2</sup> )
ÿ	Local lateral velocity of the pipe due to vibratory motion
δ	Apparent linear displacement, $\frac{1}{2}$ amplitude deflection (ft)
δ <sub>D</sub>	Deflection of pipe bottom due to drag when n <sup>th</sup> mode is excited by vortex shedding
δ <sub>T</sub>	True linear displacement, $\frac{1}{2}$ amplitude deflection (ft)
λ	Full-scale diameter/model diameter
θ	Apparent angular deflection at accelerometer (deg)
θ <sub>0</sub>	Initial amplitude
θ <sub>T</sub>	True angular deflection at accelerometer (deg)

- $\dot{\theta}$  Angular velocity (rad/sec)
- $\ddot{\theta}$  Angular acceleration (rad/sec/sec)
- $\nu$  Viscosity ( $ft^2/sec = 1.25 \times 10^{-5}$ )
- $\omega_n$  Vibratory velocity (rad/sec)

## 1. INTRODUCTION

The current concept in energy extraction from the temperature difference between ocean surface water and deep water, ocean thermal energy conversion (OTEC), requires a lengthy, large-diameter pipe (about 2000 to 3000 feet long) to reach the deep water. The pipe diameter ranges from 6 feet for proposed early test systems, to 60 or even 100 feet for large, commercial power generation systems. The pipe must be designed to resist collapsing pressures produced by water temperature and density differences, and the reduced pressure required to induce flow up the pipe. Other design considerations include the external-drag effect on the pipe due to ocean currents, and the wave-induced motions of the platform to which the pipe is attached.) Finally, the pipe must be designed with respect to strength, stability against collapse, and freedom from damaging vibration caused by wave motion, vortex shedding, and other excitation sources.

Various approaches to the pipe construction have been proposed, including aluminum, steel, concrete, and fiberglass. More recently, a flexible pipe construction involving the use of rubber-coated nylon fabric has been proposed, by Bell Aerospace Textron, New Orleans Operations. Stability and stiffness are provided by pressurization introduced between the two concentric cylindrical walls of the pipe. This concept offers numerous advantages; for example, a very low weight, with benefits in handling, shipping, deployment, and platform size; and freedom, by reason of its very low stiffness, from the motions of the platform. These advantages lead, in turn, to a reduced total system cost.

This report presents the results of a scaled flexible cold water pipe (CWP) model test program performed by Bell to demonstrate the feasibility of this flexible pipe approach. The test program (reference 1) was funded by the Naval Ocean Research and Development Activity (NORDA) under contract N00014-78-C-0759. A scale model of a length of a CWP was fabricated from lightweight elastomer-coated material, and tested in the U.S. Geological Survey (USGS) tow tank facility at the National Space Technology Laboratory (NSTL), Bay St. Louis, Mississippi.

## 2. OBJECTIVES

The test objectives were to investigate static stability and dynamic characteristics of a flexible double-wall CWP model for ocean thermal-energy applications; specifically, these were to:

- a. Determine static buckling pressures of a model double-wall flexible CWP.
- b. Determine natural frequencies, shapes, and dampings of vibration modes of the model immersed in water
- c. Determine amplitudes and frequencies of motions, and deflection due to drag, when the model was subjected to simulated ocean currents.

### 3. SCALING STUDY

#### 3.1 Model Pipe Geometry

Prior to the model design, a brief scaling study was performed to establish the model geometry and test conditions. The largest practical length-to-diameter ratio was desired to simulate full-scale CWP's. The model geometry was determined primarily by the tow tank depth, which limited model length to approximately 10 feet, and by the practical limitations in constructing a double-wall model of very small diameter. Fabrication constraints established the model minimum diameter as approximately 8.8 inches.

#### 3.2 Reynolds Number Scaling

Full-scale Reynolds numbers ( $RN = VD/v$ ) can range from  $33 \times 10^6$  for a large pipe (30-foot inside diameter, ID; 50-foot outside diameter, OD) in a high-velocity current (3.5 knots), to  $2 \times 10^6$  for an OTEC-1 size pipe (6-foot ID, 10-foot OD) in a low-velocity current (1 knot). These currents and Reynolds numbers are representative values for upper portions of pipes. Values near the bottom of pipes may be lower by as much as a factor of ten.

Model tests at velocities more than 2.5 ft/sec would have resulted in unrealistically large deflections due to drag. Such deflections could affect vortex shedding and cause unrealistic buckles due to pipe bending. Model Reynolds numbers were, therefore, limited to approximately  $0.2 \times 10^6$ . Thus, they were not representative of upper portions of full-scale CWP's, with respect to Reynolds number. However, at the maximum tow velocity (2.5 ft/sec), the Reynolds numbers of the model were near those expected near the bottom of small (10-foot OD) full-scale pipes (figure 1).

Reynolds number has no effect on static buckling which results from reduced pressure in the pipe. It also has no effect on vibration mode shapes and frequencies, because induced velocities due to oscillations at zero tow speed are small for both model and full-scale CWP's. On the other hand, drag coefficients, vortex-shedding frequencies, and vortex-shedding forces that are sources of vibration excitation are functions of Reynolds number. However, various documents, such as references 2 and 3, suggest that these Reynolds number effects do not have major effects on pipe response to vortex shedding. Reference 2 also states that good correlation has been obtained between model and full scale, with respect to vortex-shedding response, for at least one case in which Reynolds numbers differed considerably; reference 3 shows results from these tests.

It was clearly impracticable to achieve full-scale Reynolds numbers representative of most full-scale CWP's, while also simulating length-to-diameter (L/D) ratios of full-scale pipes. It was considered important to have the

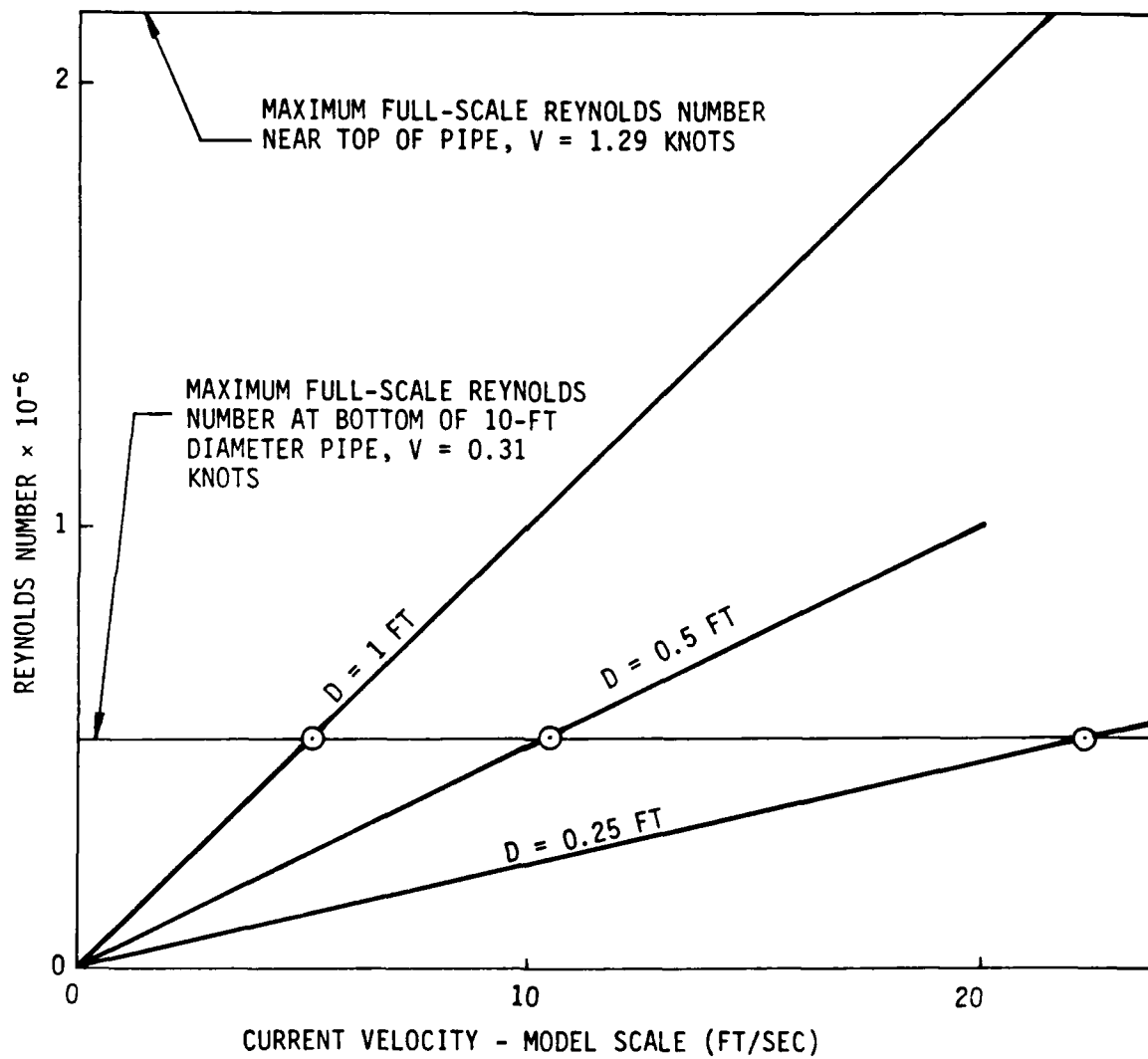


Figure 1 COLD WATER PIPE MODEL - ATTAINABLE REYNOLDS NUMBER RANGE

largest practicable L/D, which is a primary factor in determining vibration frequencies and mode shapes. Any practical increase in model diameter would have seriously degraded L/D with very little improvement in Reynolds number. Therefore, for these exploratory tests, it was necessary to test at relatively low Reynolds numbers in order to approach the scaled L/Ds and flexibilities of full-scale pipes. It is unlikely this resulted in any really significant difference in responses from those that would be observed at higher Reynolds numbers.

### 3.3 Froude Scaling

Froude scaling results in the same gravity-forces-to-inertia-forces ratio in both the model and full-scale CWP. Vibration modes and frequencies of a very flexible pipe are largely determined by this ratio. Gravity forces acting on the ballast weight produce tension in the pipe; they also produce the restoring force for pendulum modes of oscillation. Frequency equations for string-mode vibration of a pipe, depending on end conditions at the bottom of the pipe, are of the form

$$f_s = \frac{2n - 1}{4L} \sqrt{\frac{T}{u}}$$

or

$$f_s = \frac{2n}{4L} \sqrt{\frac{T}{u}}$$

where  $T$  = tension and  $u$  = mass/unit length.

If the weight of the ballast is not too large relative to the pipe weight, internal water, and effective weight of external water,  $T$  can be replaced by the ballast weight ( $W_b$ ).

The frequency equation for a pendulum mode is

$$f_p = \frac{1}{2\pi} \sqrt{\frac{W_b L}{I}}$$

where

$W_b$  = Effective weight of ballast in water

$I$  = Moment of inertia of pipe, water, and ballast about pivot point

$L$  = Length from pivot to center of gravity (cg) of ballast weight.

These facts suggest that Froude scaling may be useful for interpretation of the model vibration and tow tests for full-scale pipes. If the full-scale CWP has the same L/D as the model, Froude-scaling factors that multiply model values to obtain full-scale values are given in table I. In table I,  $\lambda$  is the result of the full-scale diameter divided by the model diameter.

If the full-scale L/D differs from the model L/D, this must also be accounted for.

Table II gives an example of scaling for a representative 30-foot-ID CWP (shown in figure 2). The range of model test pressures encompassed scaled pressures for a 30-foot pipe. Maximum tow velocities were much higher than Froude-scaled currents for this 30-foot pipe.

Table III gives scaling for a 6-foot ID pipe. Again, model pressures were representative of full-scale pressures, and maximum tow velocities were high relative to scaled current velocities.

### 3.4 Current-Velocity Scaling

Tables II and III show that test velocities to 2.5 ft/sec, within the uniform velocity field of the tow tank, were considerably higher than Froude-scaled equivalents of velocities experienced by upper portions of full-scale pipes

TABLE I  
EXAMPLE OF MODEL SCALING

MODEL	MULTIPLY BY	EXAMPLE FOR 75-FOOT-OD FULL-SCALE CWP	
		MODEL	FULL-SCALE
S/D	1	1	1
V	$\lambda^{\frac{1}{2}}$	1 ft/sec	10 ft/sec
Y	1	0.1 ft/sec <sup>2</sup>	0.1 ft/sec <sup>2</sup>
W	$\lambda^3$	13 lb	$13 \times 10^6$ lb
EI	$\lambda^5$	$22 \times 10^3$ lb-in <sup>2</sup>	$22 \times 10^{13}$ lb-in <sup>2</sup>
EA	$\lambda^3$	3700 lb/in/in	$3.7 \times 10^9$ lb/in/in
P	$\lambda$	0.2 psi	20 psi

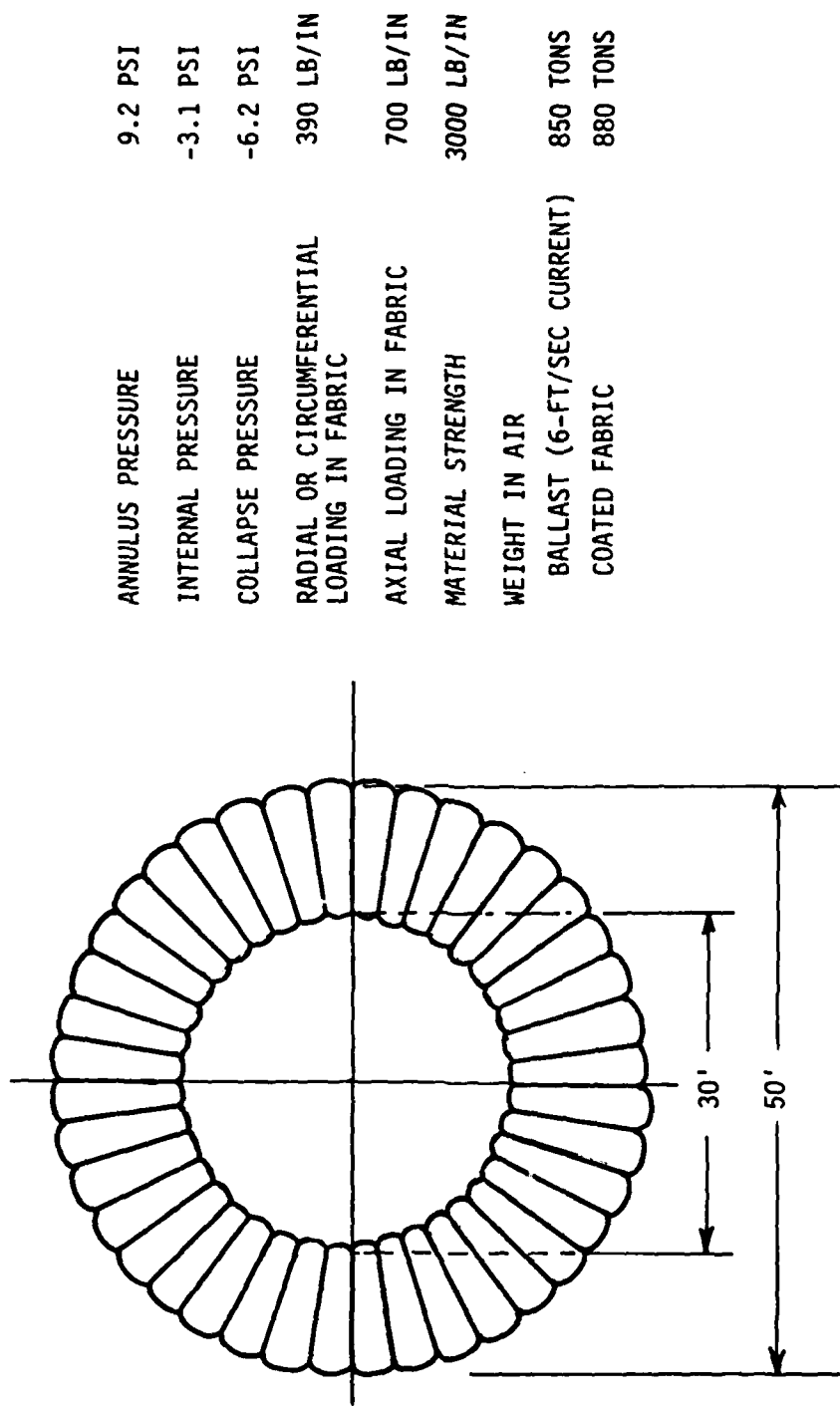


Figure 2 TYPICAL 30-FOOT-INSIDE-DIAMETER FLEXIBLE CWP

TABLE II  
SCALING TO REPRESENTATIVE 30-FOOT-ID CWP

	FULL-SCALE PIPE	FROUDE-SCALED MODEL	ACTUAL MODEL TEST RANGE
Scale Factor (Based on OD)	--	1:75	1:75
Inner Diameter (ft)	30	0.40	0.37
Outer Diameter (ft)	50	0.666	0.666
Length (ft)	3000	40	10.25
Annulus Pressure (psi) <sup>(1)(2)</sup>	19	0.25	0 to 0.82
Core Pressure (psi) <sup>(2)</sup>	-3.1	-0.04	0 to -0.16
Current Velocity (ft/sec) <sup>(3)</sup>	6	0.69	0 to 2.5
Ballast Weight in Air (lb)	$4.3 \times 10^6$	10.2	13 to 83
Maximum Reynolds Number (Based on OD)	$33 \times 10^6$	$0.05 \times 10^6$	$0.18 \times 10^6$
Bending EI (lb-in <sup>2</sup> )	$255 \times 10^{10}$	1076	22,000
Tensile EA (lb/in/in)	$81 \times 10^6$	193	3700

Notes:

(1) Annulus pressure based on 3:1 pressure ratio from model buckle tests and buckle factor of safety = 2.

(2) Model annulus pressures up to 2 psi (60 inches of water) were used for static buckle tests.

(3) Full-scale current is maximum (near surface) for operating conditions.

TABLE III  
SCALING TO REPRESENTATIVE 6-FOOT-ID CWP

	FULL-SCALE PIPE	FROUDE-SCALED MODEL	ACTUAL MODEL TEST RANGE
Scale Factor (Based on OD)	--	1:16.2	1:16.2
Inner Diameter (ft)	6.0	0.37	0.37
Outer Diameter (ft)	10.8	0.666	0.666
Length (ft)	2000	123	10.25
Annulus Pressure (psi) <sup>(1)(2)</sup>	6.6	0.41	0 to 0.82
Core Pressure (psi) <sup>(2)</sup>	-5.1	-0.19	0 to -0.16
Current Velocity (ft/sec) <sup>(3)</sup>	2.2	0.55	0 to 2.5
Ballast Weight in Air (lb)	500,000	118	13 to 83
Maximum Reynolds Number (Based on OD)	$1.05 \times 10^6$	$0.04 \times 10^6$	$0.18 \times 10^6$
Bending EI (lb-in <sup>2</sup> )	$0.29 \times 10^{10}$	2600	22,000
Tensile EA (lb/in/in)	$2.0 \times 10^6$	470	3700
Notes:			
(1) Annulus pressure based on early buckle predictions with factor of safety = 2.			
(2) 0.0361 psi = 1 inch of H <sub>2</sub> O; larger pressure ranges were used for buckle tests.			
(3) Current is maximum, near surface, for operating conditions.			

in an ocean current. In addition, ocean currents may differ by a factor of 4 to 10 from the bottom to the top of the CWP. With such current gradients, vortex-shedding frequencies are unlikely to correlate with pipe motion frequencies over more than a fraction of the pipe length. Figure 3 illustrates this effect. In fact, with the current profile of figure 3, the two lowest vibration modes of this OTEC-1 pipe have frequencies so low that they probably would not be excited. Therefore, the tests with a uniform velocity field and high velocities were quite severe relative to full-scale environments.

### 3.5 Ballast-Weight Scaling

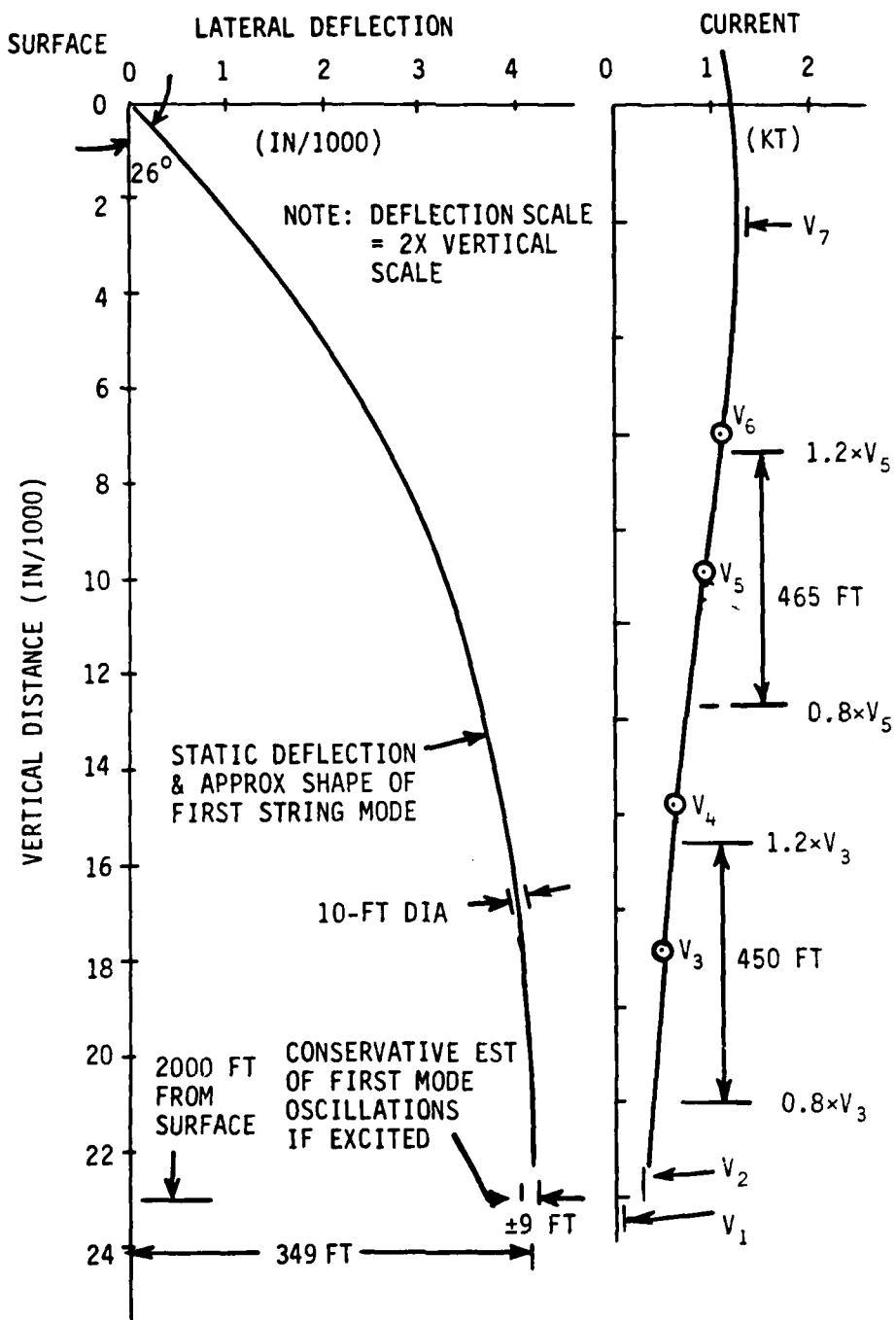
Full-scale ballast weights will depend on the criteria for lateral and/or vertical deflections of the flexible CWPs, the current profiles for which they are designed, and possibly on criteria to prevent buckling due to current. Thus, the  $4.3 \times 10^6$ -lb ballast weight shown in table II is representative, but may either increase or decrease for later designs. The 13-pound minimum ballast used for the model tests was 27 percent higher than the scaled ballast weight for this 30-foot-CWP design. This minimum model ballast weight was the weight of the ballast can without added weights. The can was sized so that large weights could be inserted, for tests over a large ballast range, without changing the total model length nor its drag characteristics.

The model ballast weights were less than the scaled value corresponding to a ballast for a smaller full-scale pipe. A Bell preliminary design for OTEC-1 (6-foot ID  $\times$  2000 feet long) had a 500,000-pound ballast (table III). The model Froude-scaling factor was  $6 \text{ ft}/0.37 \text{ ft} = 16.2$ . The Froude-scaled model ballast for this configuration would be 118 pounds. Tests were conducted with ballasts of 13, 36, and 83 pounds.

Because of the desire to search for potential problems and to obtain data trends, rather than to simulate a specific full-size configuration, both model ballast and pressure were varied over wide ranges. Results can be interpolated or extrapolated for application to specific full-size CWPs. In doing this, however, the relatively low L/D of the model should be considered. There will also be some effects if the cross section of the full-scale pipe is not geometrically similar and/or if material elastic characteristics are much different than scaled model values.

### 3.6 Model Material Stiffness

Another consideration in model design and testing was the material tensile stiffness ( $E$ ,  $\frac{\text{lb}}{\text{in}^2} : \frac{\text{in.}}{\text{in.}}$ ; or  $E' = \text{pli/in/in}$ ) of the model material relative to full-scale material. For a given cross-section geometry and size, the material tensile stiffness determines axial (EA) and bending (EI) stiffnesses. Experience with scaling of surface effect vehicle seals had shown that model materials generally have higher than desired tensile stiffnesses. The same



NOTE: CIRCLED POINTS INDICATE WHERE  $V_N$  IS CURRENT VEL AT WHICH STROUHAL FREQ = NATURAL FREQ OF  $N^{th}$  STRING MODE

Figure 3 LENGTHS OF PIPE WHERE VORTEX FREQUENCIES MATCH STRING MODE FREQUENCIES

situation existed for the double-wall CWP model. Therefore, the material selected had the lowest stiffness of the readily available, adequately strong materials. Still, the selected material was stiffer than desired, as indicated by EI and EA values in tables II and III. Calculations indicated this would have little effect on static ring buckling test results (cross-section change due to reduced internal pressure), since ring buckling depends on the annulus ring stiffness (controlled by pressure forces rather than material characteristics).

However, the higher than desired stiffness also resulted in buckling at the top and near middepth of the model, due to bending moments from drag or bending oscillations, when such buckling would not be expected in a full-scale pipe. This is because buckling, due to drag or vibratory oscillations, occurs when deflections or pipe bending produce positive or negative strains which exceed the axial strains due to axial loads produced by the ballast weight and annulus pressure. These deflections ( $\delta$ ) are limited more by the ballast restoring moment than by EI, and a high EA results in low axial strains. Thus, the axially stiff model will buckle near its support at lower values of  $\delta/D$  than will a full-scale pipe with lower EA. For a given  $\delta/D$ , the low L/D model will buckle, when a higher L/D full-scale pipe will not. Also, the model was tested at velocities which produced maximum values of  $\delta/D$ , much greater than would occur with a full-scale CWP.

The relatively high EA of the model, together with its low L/D, made it unlikely that useful results could be obtained from tests of heave characteristics, or pressure and/or cross-section changes due to waves. Therefore, heave and wave response tests were not attempted.

The model EI values in tables II and III were 8.5- and 20-times scaled values for the 6- and 30-foot pipes, respectively. Such large factors could be significant if EI and tensile forces due to ballast and pressure were equally important in determining full-scale pipe vibration modes and frequencies. However, if EI for a full-scale pipe contributed only 1 percent of the total effective stiffness (due to both EI and axial tensions), an increase by a factor of 20 in EI would only increase total effective stiffness by about 20 percent, and would increase natural frequencies by only about 10 percent. It is difficult to make quantitative assessments of the relative effects of EI-versus-tension loads without calculations of frequencies and mode shapes which include combined effects. For lower modes of full-scale pipes, EI effects are insignificant. Because of the  $1/L^2$  term in beam frequency equations versus  $1/L$  in string mode equations, EI becomes relatively more important for low-L/D configurations and the model.

Regardless of the significance of the model EI-versus-tension effects, their combined effects were determined in the vibration tests. These frequencies were varied over a wide range by changing ballast weights and pressure. The lack of any unexpected results in the subsequent tow tests, with similar ballast and pressure ranges, gives at least a reasonable assurance that there

are no basic feasibility questions associated with vortex excitation of flexible CWP modes. Tests of higher-L/D models would be desirable to develop further confidence. However, as discussed later, there are major limitations on high-L/D-model tow tests.

### 3.7 Application of Model Results to Full Scale

With the many deviations from ideal scaling, it might appear that only limited information could be obtained from testing this model. However, the deviations from ideal scaling are of little significance for the static ring buckling tests. (Reynolds number is not a factor in the static ring buckling tests, L/D is a secondary factor, and the material elongations only cause second-order effects.) Therefore, the annulus-pressure-to-core-pressure ratio, when cross-section buckling or ovaling occurs, would be essentially the same for model and full-scale pipes with geometrically similar cross sections. Designs with different cross-section geometry (eg, ratio of inner to outer diameter) could have quite different pressure ratios at the buckle boundary. Therefore, results of these tests are directly applicable only to full-scale CWPs with geometrically similar cross-section geometries.

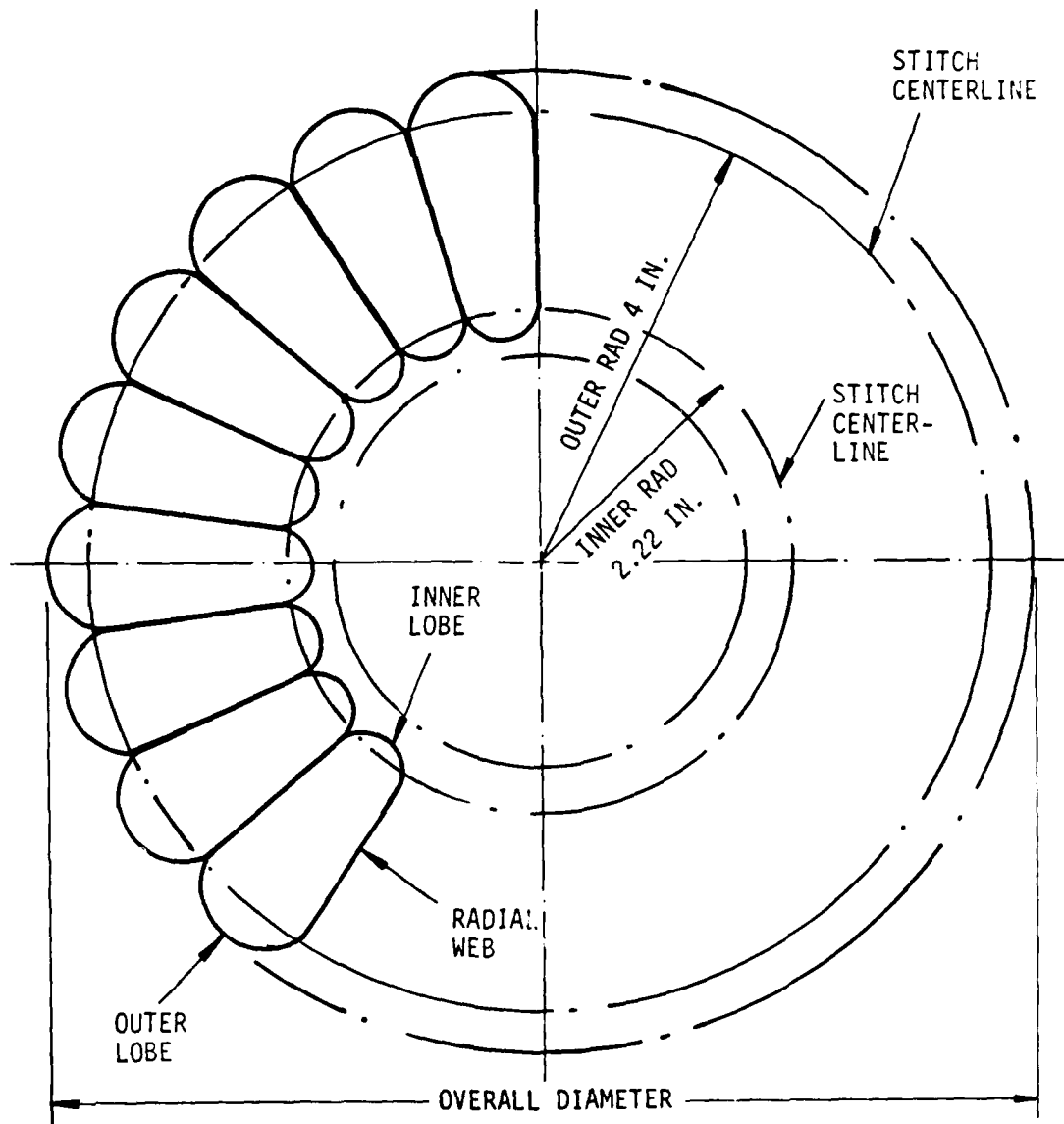
It was recognized that interpretation of model vibration and tow-test results, and/or application to full-scale pipes, would be less straightforward than use of the static cross-section buckling test results. However, it was believed that, because of the unique characteristics of these very flexible pipes, some exploratory tests were desirable even if scaling was not ideal. As a minimum, these tests would help establish whether or not such pipes have any unanticipated characteristics, and, by varying parameters such as ballast weight and pressures, trends could be established for possible subsequent comparison with predicted model characteristics. Also, the vibration and tow tests would provide low-cost model construction, instrumentation, and testing experience that would be valuable for possible future tests of other models.

#### 4. MODEL DESCRIPTION

From the scaling considerations, and others to be discussed in section 9, a nominal model size of an 8-inch-outside-seam diameter and a 4.44-inch-inside-seam diameter was selected. The basic model particulars are given in table IV with a diagram of the cross section in figure 4.

Figures 5 and 6 are photographs of the model component parts (an aluminum header section, the flexible pipe, and the lower ballast section), and significant material particulars are given in table V. The main dimensions are shown in figure 7, and the assembled pipe during the air-inflation check is shown in figure 8. The model flexible CWP was fabricated from a urethane-coated nylon fabric (for basic characteristics see table V). All radial webs were sewn to the inner and outer lobes. All seams were sealed externally, and additional coats of sealant were applied to all inner pipe seams and joints. The ends of the flexible-CWP lobes were secured to the metal end sections with pipe clips. For ease of model fabrication, the radial web ends were not secured to the end fittings.

In order to determine the natural frequencies, a pulsed jet water system was attached to the model. A system schematic is shown in figure 9 and component parts in figure 10. The system consisted of two diametrically opposed water hoses attached to the lower end of the pipe. The lower ends of the hoses were capped off, and short lengths of Tygon tube were attached to provide jets normal to the pipe axis. The jets were alternately actuated through electric valves by microswitches and cams driven by a variable-speed dc motor. The cams were circular wood disks with sections of half-round dowels attached around the circumference. Cam I provided 9 cycles per revolution and cam II 18 cycles per revolution. This system was removed for tow tests.



NOTE: OVERALL DIAMETER MEASURED DURING THE TESTS = 9.25 IN.

Figure 4 GEOMETRY OF MODEL

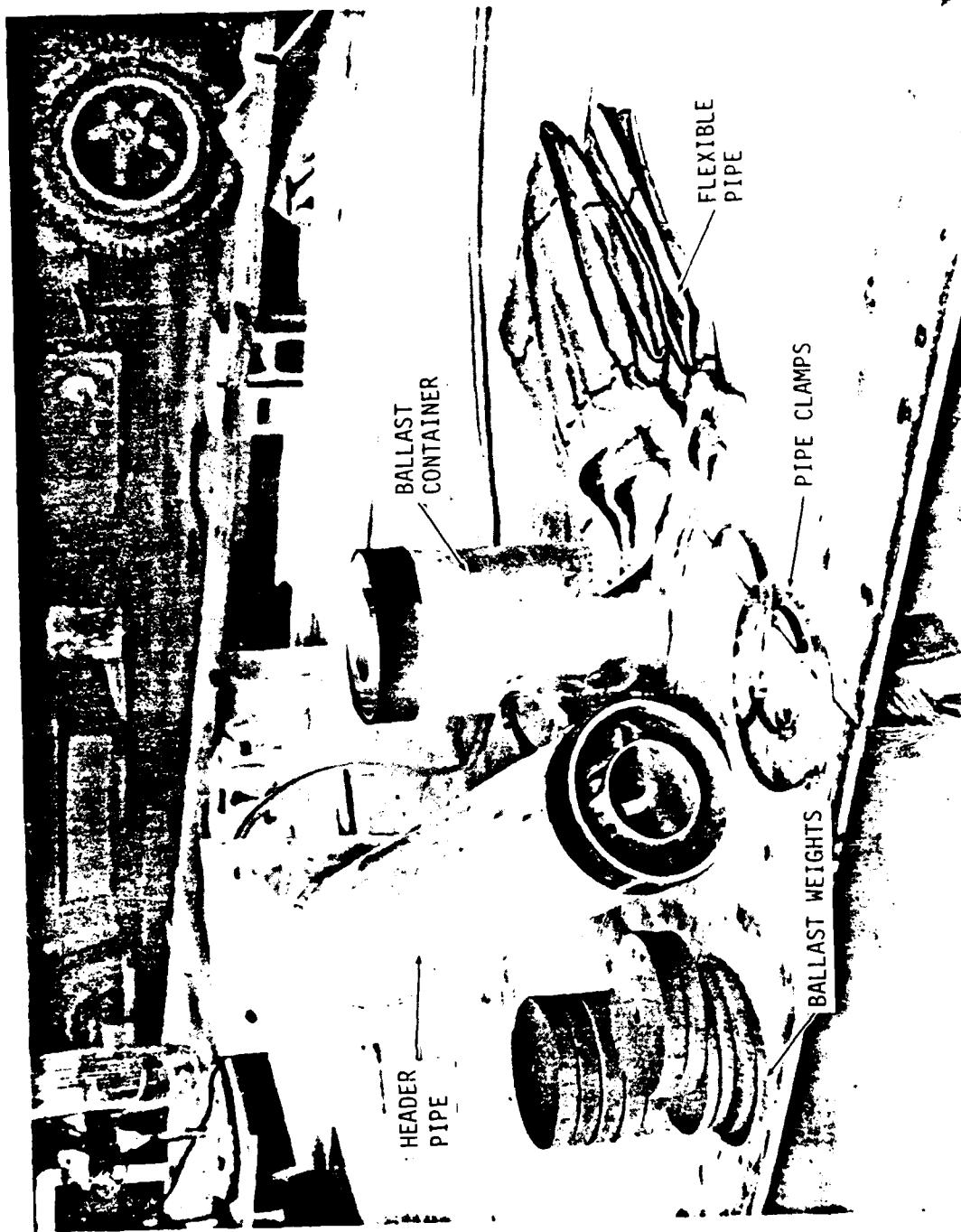


Figure 5 CWP MODEL COMPONENTS



Figure 6 INSIDE VIEW OF CWP MODEL

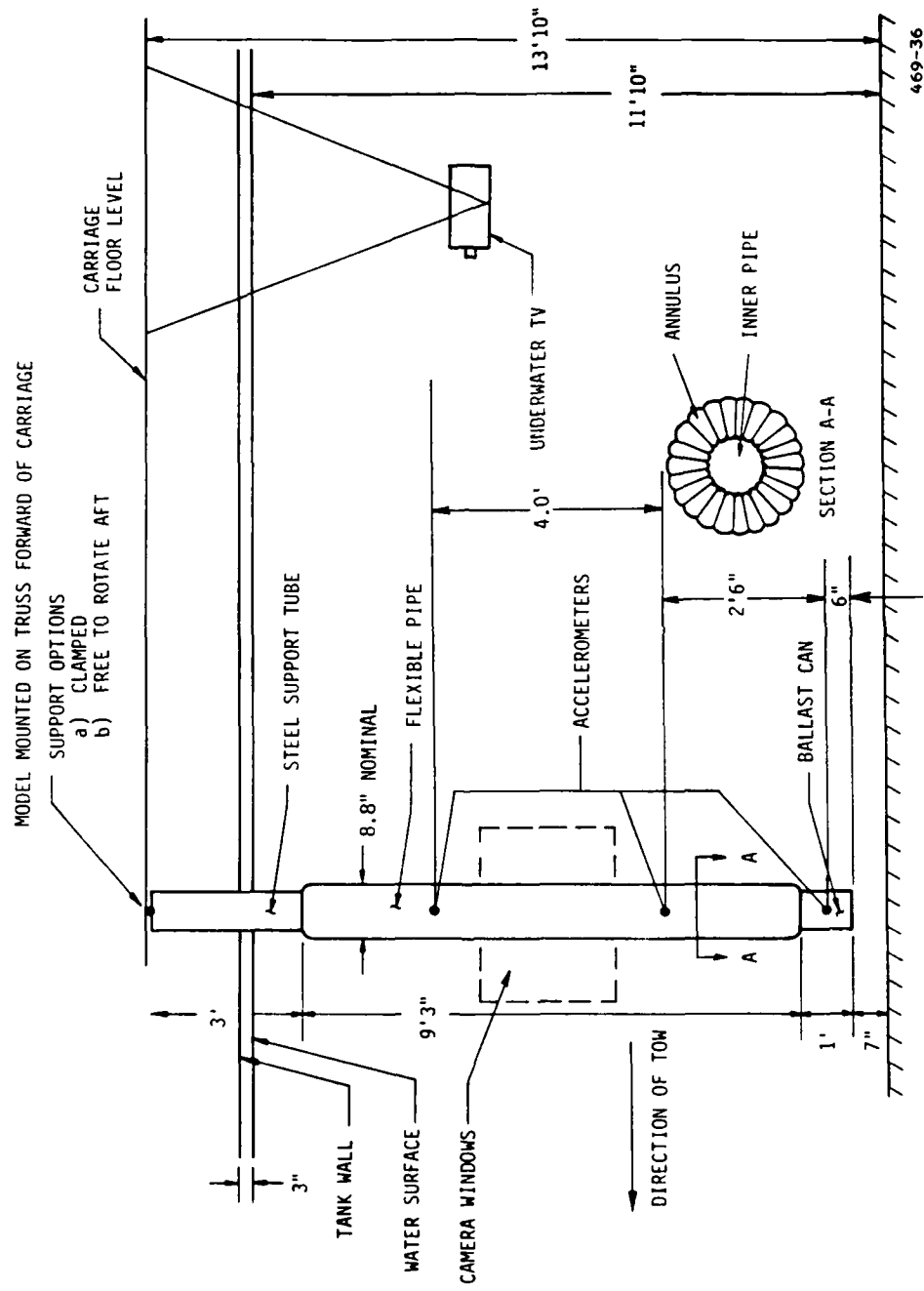


Figure 7 SCHEMATIC OF FLEXIBLE CWP MODEL IN TOW TANK

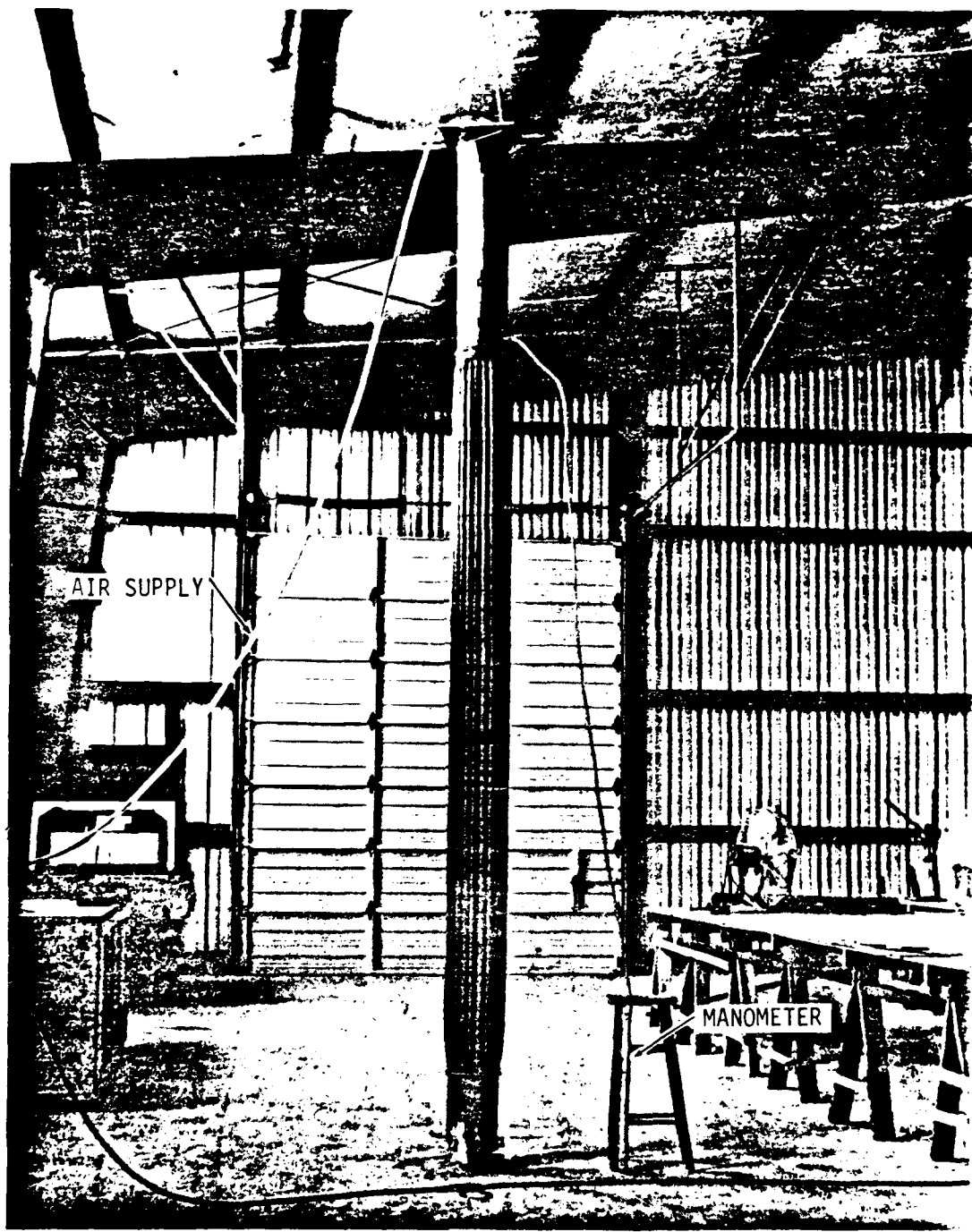


Figure 8 ASSEMBLED CWP MODEL DURING AIR-INFLATION CHECK

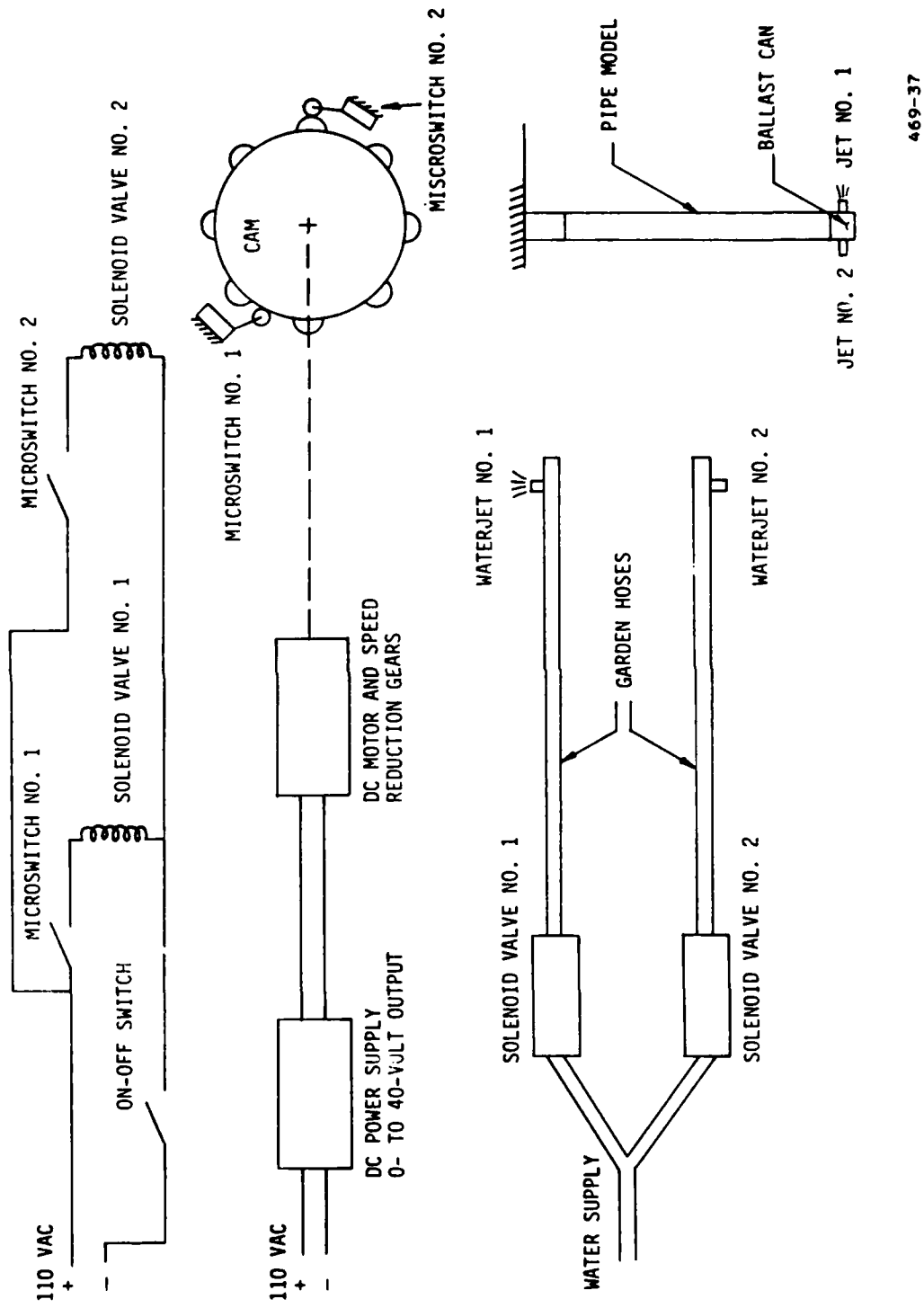


Figure 9 SCHEMATIC OF PULSED JET SYSTEM FOR VIBRATION TESTS

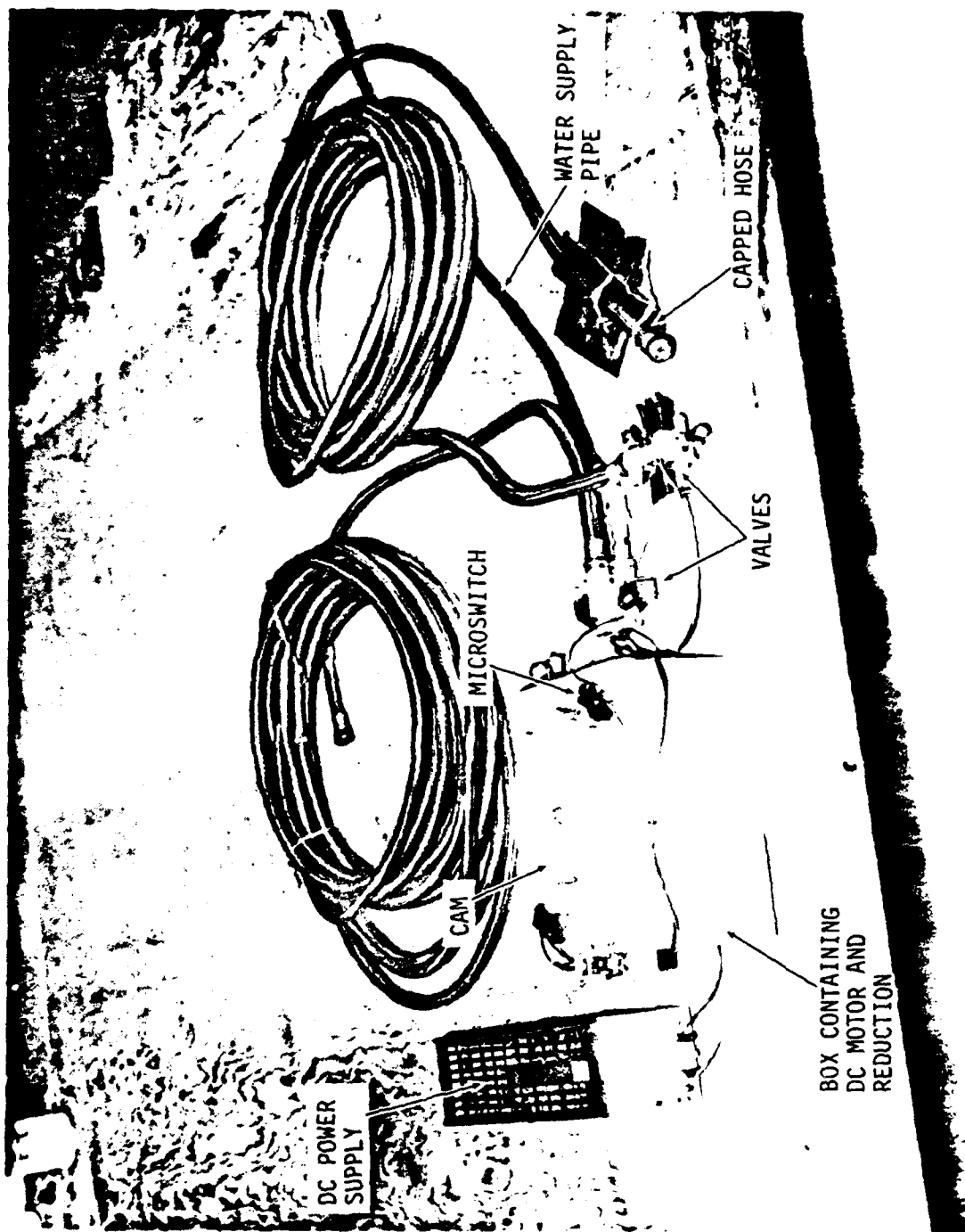


Figure 10 PULSED WATERJET SYSTEM

TABLE IV  
MODEL PARTICULARS

Pipe Length	9.25 ft
Number of Radial Webs	22
Annulus Cross-Section Area	44.2 in
Ballast Load	Up to 83 lb
Inflated Outer Radius (see figure 4)	4.00 in*
Inflated Inner Radius (see figure 4)	2.22 in.
Outer Lobe Radius	0.59 in
Lobe Length (Outer)	1.53 in
Inner Lobe Radius	0.36 in
Lobe Length (Inner)	0.78 in
Radial Web Length	1.78 in
Pipe Cross-Section Material Length	90.00 in

\*Overall outside diameter measured on model = 9.25 inches.

TABLE V  
SIGNIFICANT MATERIAL PARTICULARS

Style Number	Korathane 5056
Supplier	Incopa Industries
Color	Yellow
Yarn	70-Denier Nylon
Weave	Taffeta
Count Picks/Inch (Warp and Fill)	104 x 88
Fabric Weight	1.6 oz/yd <sup>2</sup>
Coating	Eurethane
Sides Coated	Single
Total Weight	2.6 oz/yd <sup>2</sup>
W x F Tensile Strength	100 x 90 lb/in

## 5. FACILITY AND INSTRUMENTATION

The USGS tow tank facility located at NSTL was used for the tests. An existing aluminum cantilevered frame was used to support the model CWP from the carriage floor. During tow tests, two pillow bearing blocks, located on the frame, allowed the model only fore and aft rotational freedom of movement. Rotational freedom was removed for the vibration tests, and no lateral rotation of the support was permitted during the tow tests. The general arrangement of the model in the tank is shown in figure 7. Three Entran EGC-240-5, 5g accelerometers were attached to the model, and their output was recorded on a seven-channel Ampex PR-1300 magnetic tape recorder and a Hewlett-Packard Co. 74-18, eight-channel oscilloscope recorder. The accelerometer natural frequencies were nominally 370 Hz. The locations of the accelerometers are shown in figure 7. The nominal weight of each accelerometer was 4 grams, which is very light relative to the weight of water in the pipe core and annulus (~220 pounds). Manometers were provided to measure the annulus and core pressures, and these were recorded manually.

An underwater television camera and videotape recorder were used, initially from a tankside window, for the vibration and static buckling tests. During the tow tests, the TV camera was supported from a boom astern the model.

In order to measure the CWP deflection due to drag, the model was fitted with a target projecting aft from the ballast can. The position of the target was sighted from the carriage through a length of tubing during the two tests. The sighting tube was supported on a movable wooden frame incorporating a measuring scale from which its locations were recorded. Figure 11 is a general view of the tow carriage, and figure 12 shows the model under test.



Figure 11 GENERAL VIEW  
OF TOW CARRIAGE



Figure 12 MODEL UNDER TEST

**6. RANGE OF TESTS**

Tests were carried out for a range of ballast weights and for a range of pipe annuluses and core pressures. Three test phases were performed as follows:

- a. Static ring buckling tests
- b. Natural frequency tests
- c. Tow tests.

The test runs are summarized in table VI.

**TABLE VI**  
**SUMMARY OF TESTS**

BUCKLING						
RUN NUMBER	BALLAST WEIGHT (LB)	PRESSURE RANGE	$P_{\text{ANNULUS}}^*$ (IN. H <sup>2</sup> O)	$P_{\text{CORE}}^*$ (IN. H <sup>2</sup> O)	COMMENTS	
1	13	Low	3.0	-1.2	Buckle noted	
2	13	Low	9.9	-3.2	Buckle noted	
3	13	Low	15.3	-5.0	Buckle noted	
4	36	Low	9.7	-2.8	Buckle noted	
5	36	High	25.0	-8.0	Buckle noted	
6	36	--	--	--	Run 5 repeated	
7	36	High	55.8	-18.4	Buckle noted	
VIBRATION						
RUN NUMBER	BALLAST WEIGHT (LB)	PRESSURE RANGE	$P_{\text{ANNULUS}}^*$ (IN. H <sup>2</sup> O)	$P_{\text{CORE}}^*$ (IN. H <sup>2</sup> O)	CAM	COMMENTS
8	36	Low	8.6	-2.0	II	Some indication of 2nd mode vibration
9	36	Low	4.8	0.3	I	
10	36	High	18.0	-4.0	I	
11	13	Low	0.5	0.0	I	
12	13	Low	1.2	0.0	II	
13	83	Low	1.8	0.0	II	Some indication of 2nd mode vibration
14	83	Low	1.8	0.2	I	
15	83	High	18.0	-4.5	I	

\*Nominal

TABLE VI (Cont)

TOW						
RUN NUMBER	BALLAST WEIGHT (LB)	PRESSURE RANGE	P <sub>ANNULUS</sub> * (IN. H <sup>2</sup> O)	P <sub>CORE</sub> * (IN. H <sup>2</sup> O)	MAXIMUM VELOCITY (FT/SEC)	COMMENTS
16	13	Low	1.6	1.0	1.805	Local buckling at top of pipe, trailing side
17	13	High	22.8	-4.0	0.703	
18	13	Low	1.2	1.3	0.425	Added spoilers
19	36	Low	1.4	1.3	1.310	
20	83	High	18.0	-4.0	2.500	2nd mode vibration
21	83	Low	1.9	-0.7	2.020	2nd mode vibration

\*Nominal

## 7. DATA REDUCTION

Data reduction for static ring buckling tests consisted of plotting annulus pressure versus core pressure, as read from the manometers.

Data reduction for vibration and tow tests mainly involved accelerometer measurements. The accelerometers consisted of a mass supported by a strain-gaged cantilevered plate, with the strain gages arranged to measure bending moment in the plate. This arrangement acts like a pendulum and, where the actual oscillatory acceleration levels are low in relation to gravity, the accelerometers measure angular displacement. The static outputs of the accelerometers, and the data system, were calibrated against angular displacement of the sensitive axis from the horizontal. The results are shown in figure 13. With the gains used for most tests, a full-scale traverse of the oscillograph scale for the bottom accelerometer represents a static angle change of  $\pm 6$  degrees. For a few tests where pipe motions were large, signals were rescaled by a factor of 2. Full scale for the bottom accelerometer then represented a  $\pm 12$  degree change. Full-scale deflections of oscillograms from the upper and middle accelerometers represented 11-percent-larger angles.

When the model oscillated laterally in a pendulum mode, with the pipe acting essentially as a rigid body pivoted near its upper end, the oscillograph trace deflections consisted of two components. At the times of maximum oscillatory deflection,

$$N = \frac{g \sin \theta_T - (2\pi f)^2 \delta}{g},$$

which for small angles is approximately

$$N = \frac{\theta_T}{57.3} - \frac{(2\pi f)^2 \delta}{g}$$

where

N = The accelerometer output (g)

$\theta_T$  = The true angular deflection at the accelerometer (deg)

$\delta$  = The lateral linear (or arc length) deflection at the accelerometer (ft)

f = Frequency of oscillation (Hz)

g = Acceleration of gravity (32.2 ft/sec<sup>2</sup>).

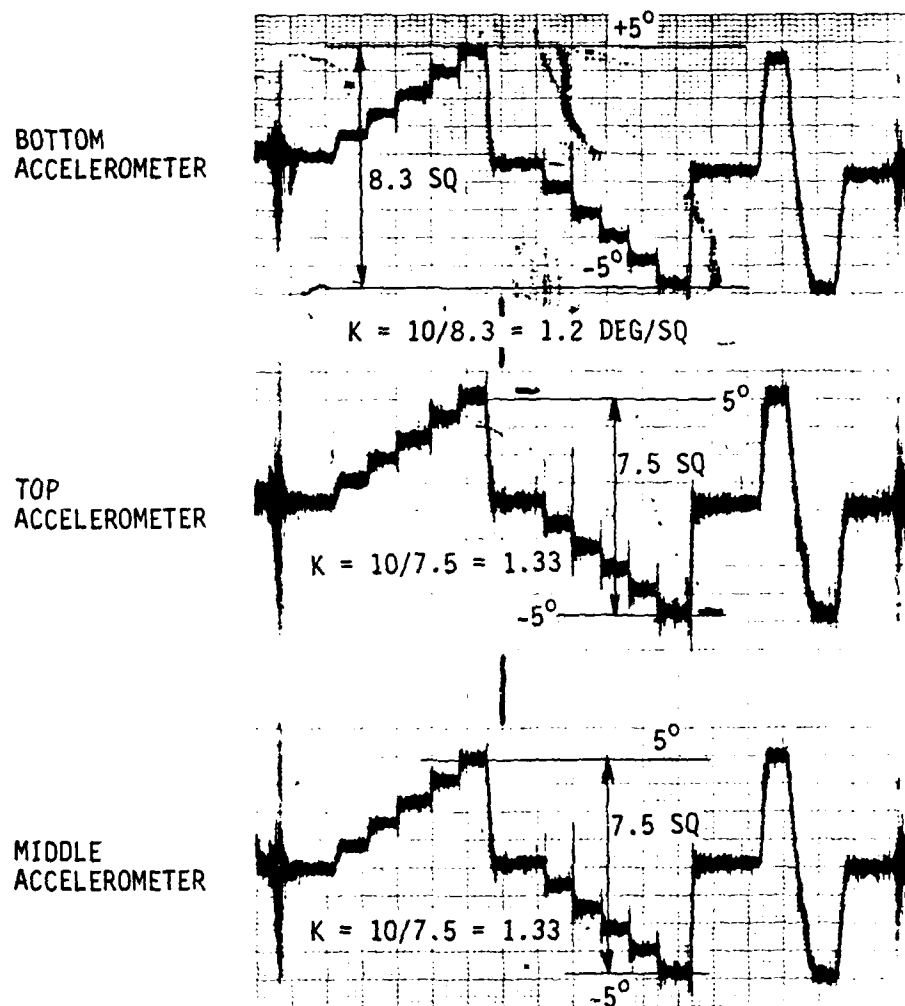


Figure 13 ACCELEROMETER CALIBRATION

If  $\theta$  is the apparent or approximate angular deflection (in degrees) that would be obtained by applying the static calibration factor  $K$  degrees per square on the oscillogram, then for the pendulum mode,  $\delta = l\theta/57.3$  deg/radian, and  $\theta = 57.3$  deg/radian  $\times N$ . It can be shown that for these cases  $\theta_T = \theta(1 + 1.23lf^2)$  where  $l$  = distance from the apparent pivot point to the accelerometer. Figure 14 shows this correction factor  $(1 + 1.23lf^2)$  for each accelerometer.

Vibration and tow response  $\delta/D$  curves in this report do not include these  $\delta$  corrections, which are functions of accelerometer position and frequency. The simplified data reduction used for the response curves to expedite the data presentation is outlined below. Basic trends shown by the resulting figures would not be altered by making the corrections. Where such corrections might be significant, they are noted or discussed.

The fact that the accelerometers sensed a gravity component that was the same order of magnitude, and generally greater than, accelerations due to the dynamic oscillations contributed to difficulties in measuring responses of higher oscillation modes. Unless the relationship between  $\theta$  and  $\delta$  is known, it is not possible to determine the individual  $\theta$  and  $\delta$  contributions to the accelerometer outputs.

From the above equations, it can be shown that for the model pendulum mode, the  $\delta$  component predominates if the measured frequency is much less than

$$f_p = \frac{1}{2}\pi \sqrt{\frac{g}{l}} ,$$

which is the frequency of a simple pendulum of length  $l$ . The  $\delta$  component predominates if  $f$  is much greater than  $f_p$ . For the upper, middle, and lower accelerometer locations,  $f_p = 0.5, 0.335$ , and  $0.289$  Hz.

A typical oscillograph record taken during the tests is shown in figure 15. During most vibration and tow tests, the CWP model acted as a pendulum rotating about a point near the metal header section. From the oscillograph scale readings and the length of the pipe plus ballast can, the approximate lateral deflection at the ballast can bottom, as a proportion of pipe diameter, was computed as outlined below.

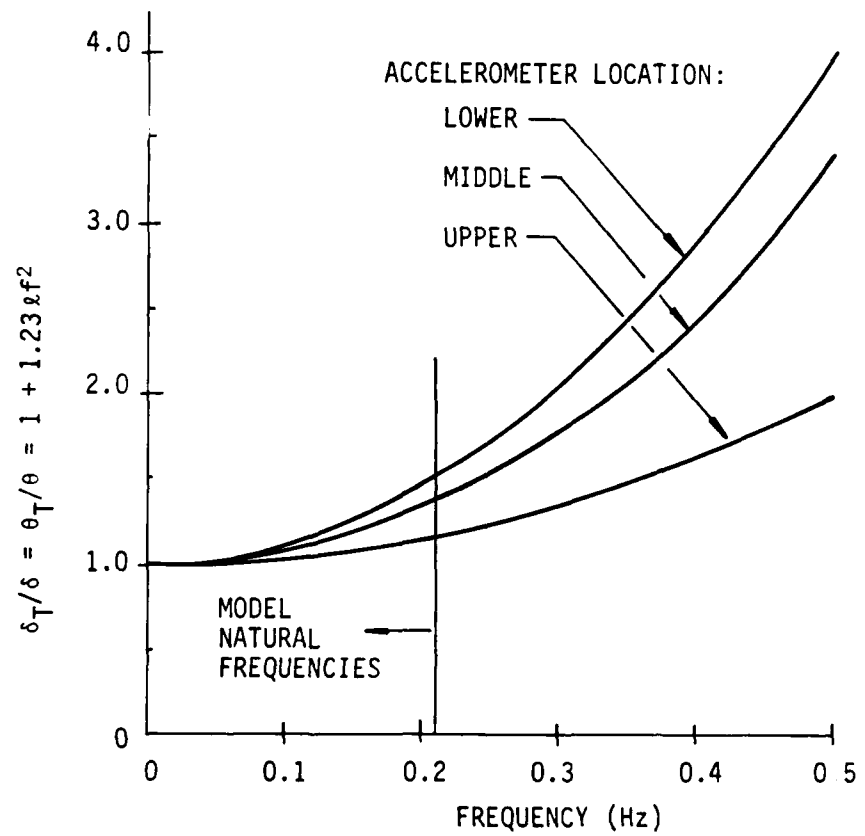


Figure 14 PENDULUM MODE AMPLITUDE CORRECTION FACTORS

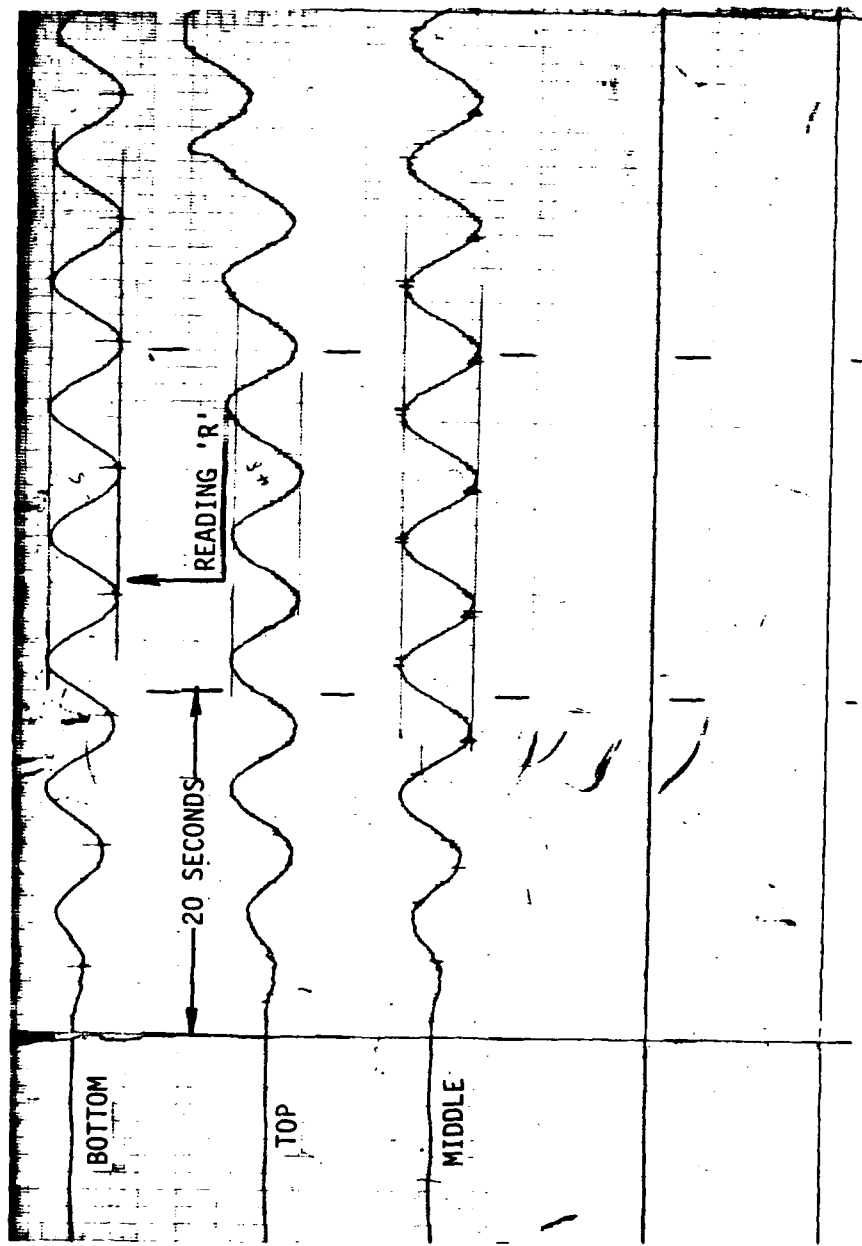


Figure 15 TYPICAL OSCILLOSCOPE RECORD: RUN 9-5

### 7.1 Lateral Displacement Computation

The following equations and the sketch below were used in lateral displacement computation:

$$\delta = (R/2) \times K \times (L/57.3)$$

$$\frac{\delta}{OD} = \frac{(R/2) \times 1.2 \times (10.25/57.3)}{0.75} = 0.1431R$$

where

$\delta$  = One-half amplitude deflection (ft)

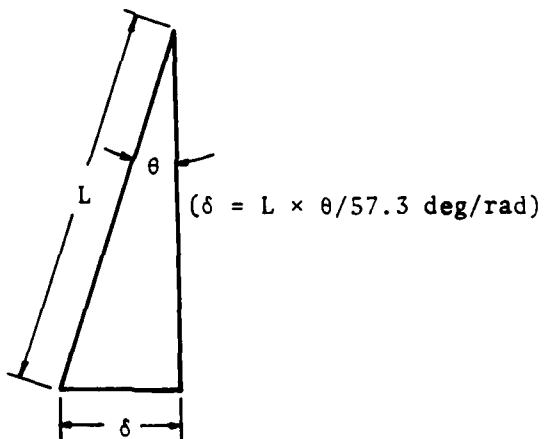
OD = Pipe outer diameter (0.75 ft)

K = Calibration factor (1.2 deg/square)

R = Bottom accelerometer reading (peak-to-peak) squares on record

L = Length of pipe plus ballast can (10.25 ft).

Measurements of frequency were also obtained from these records against the known time base.



## 8. RESULTS

### 8.1 Static Ring Buckling Tests

The results of the static ring buckling tests are graphically illustrated in figures 16 and 17, which show the variation of annulus pressure with core pressure, each given in inches of water. The tests were carried out at various initial annulus pressures (from 3 to 52 inches) and at two ballast conditions (13 and 36 pounds).

The test procedure first established a nominal annulus pressure, and set the core pressure at zero with respect to the free-surface water level. Water was then pumped out of the core and observations made of the pipe shape. The onset of change in pipe shape coincided with an increase in annulus pressure; as can be seen from figures 16 and 17, this occurred when the core pressure reached a negative value of 1/3 the annulus pressure. Collapse occurred by a gradual ovaling and flattening of the pipe cross section. In the collapsed mode, the pipe section appeared to become elliptic and similar to the sketch shown in figure 18.

### 8.2 Vibration Tests

For these tests, the model was located near a tow tank window and cantilevered from the support frame attached to the carriage.

The vibration tests results are shown in figures 19 through 22. These figures show the variation of pipe amplitude, at the ballast can bottom, with forcing frequency. Figure 19 illustrates the results with 13-pound ballast weight. A maximum one-half amplitude of 1.5 diameters at a natural frequency of 0.075 Hz was observed.

Figure 20 shows the results with a 36-pound ballast. This shows a maximum one-half amplitude of approximately 0.5 diameter at a natural frequency of 0.17 Hz with a high annulus pressure, and a low-pressure natural frequency of 0.13 to 0.14 Hz with somewhat larger amplitudes. Results are also shown in this figure for an annulus pressure of 8.6 inches of water and a core pressure of -2.0 inches of water (run number 8). This data was obtained using cam II, which provided 18 pulse-jet cycles per revolution. It is felt that the low response in this case was a result of insufficient off time between the on times of the pulsed-jet water system using this cam.

The results for the 83-pound-ballast condition are given in figure 21, and show natural frequencies of 0.18 and 0.21 cycle per second for the high and low pressure, respectively. Amplitudes are less than for lower-ballast cases.

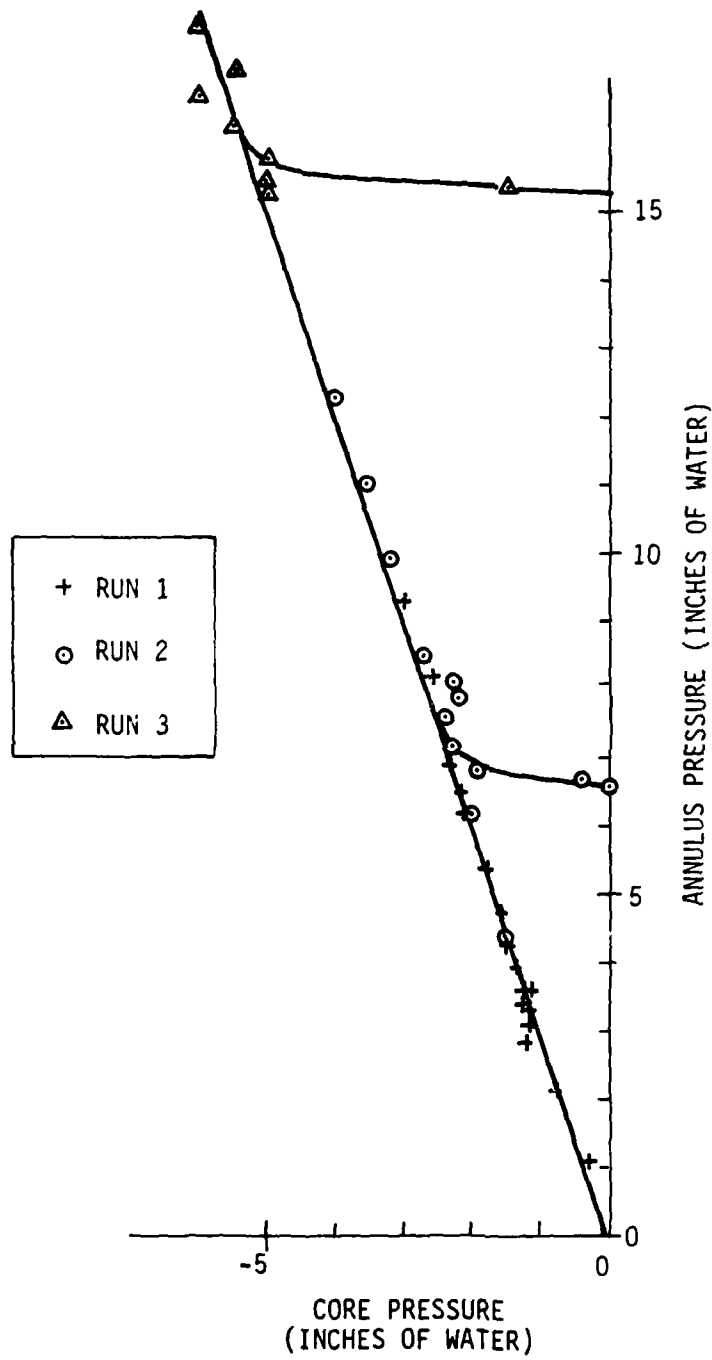


Figure 16 VARIATION OF ANNULUS PRESSURE WITH REDUCED  
CORE PRESSURE (BALLAST WEIGHT, 13 LB)

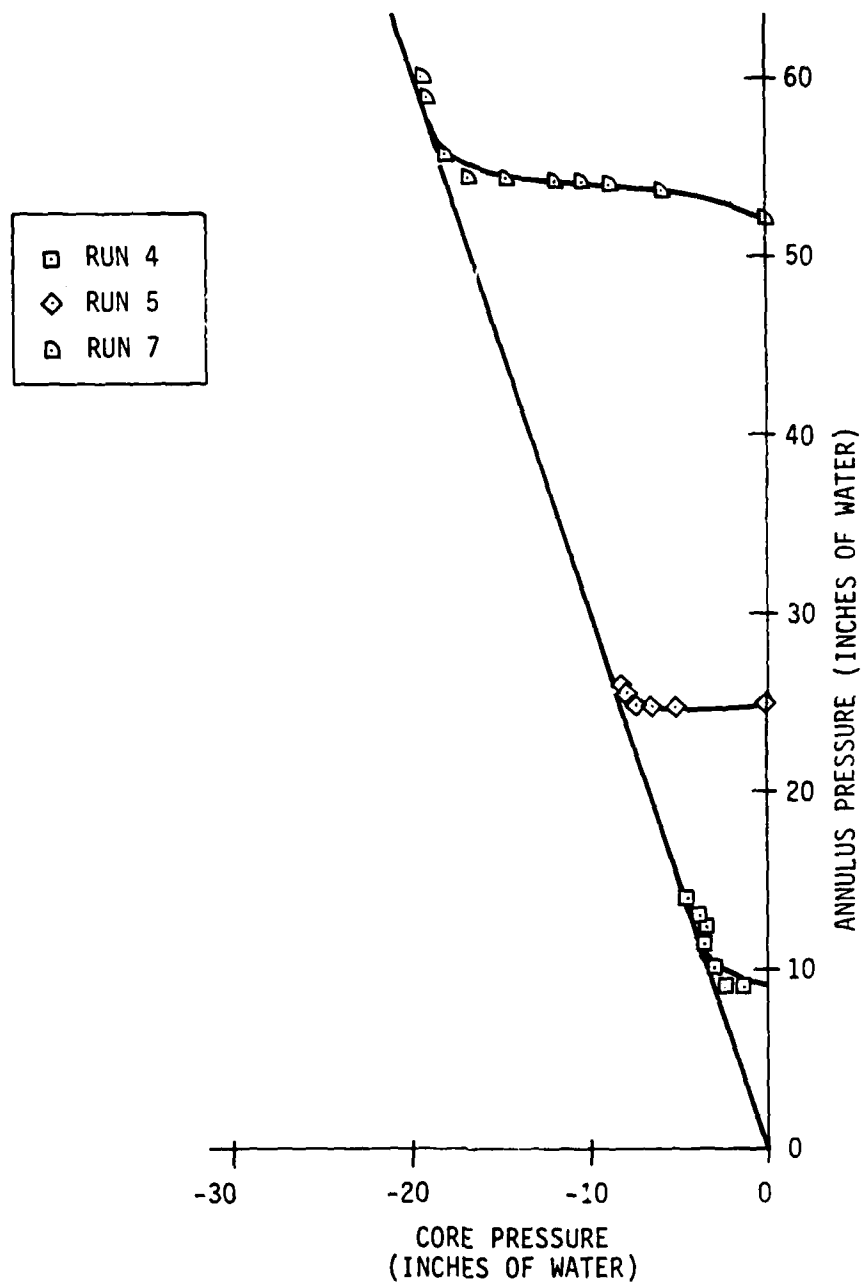


Figure 17 VARIATION OF ANNULUS PRESSURE WITH REDUCED  
CORE PRESSURE (BALLAST WEIGHT, 36.05 LB)

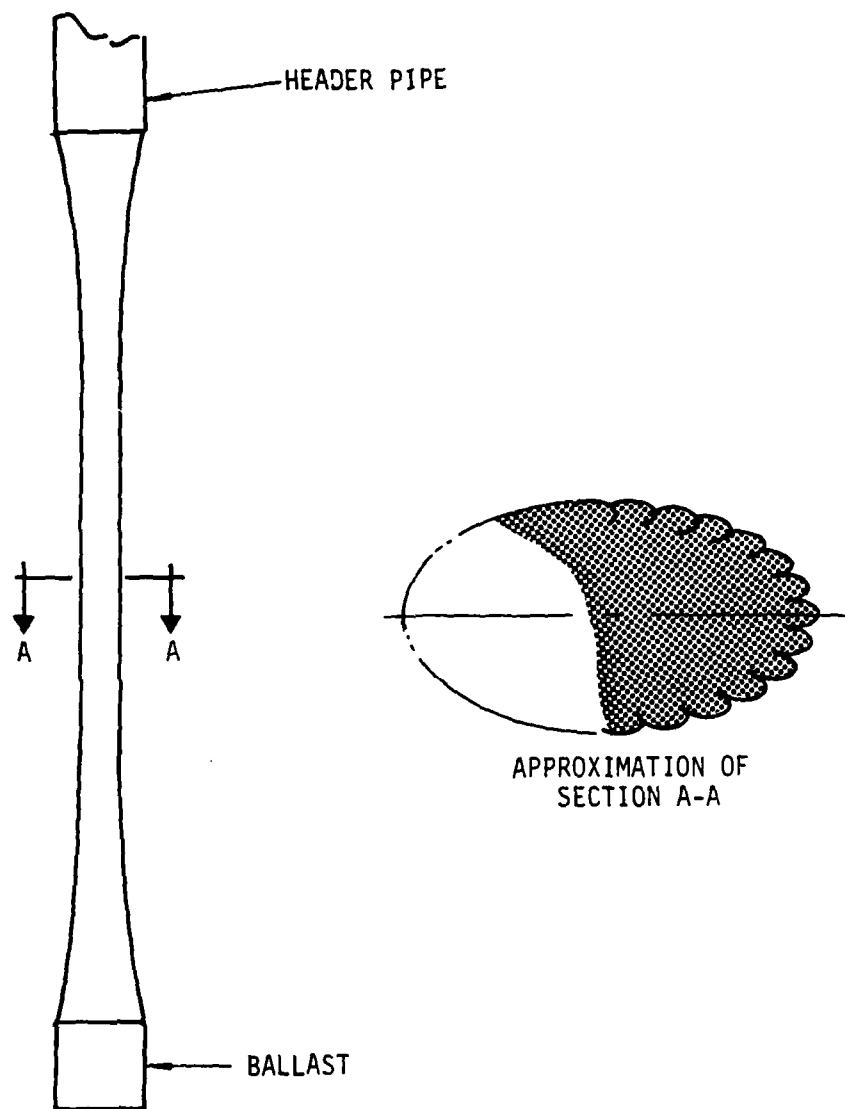


Figure 18 APPROXIMATE GEOMETRY  
OF COLLAPSED PIPE

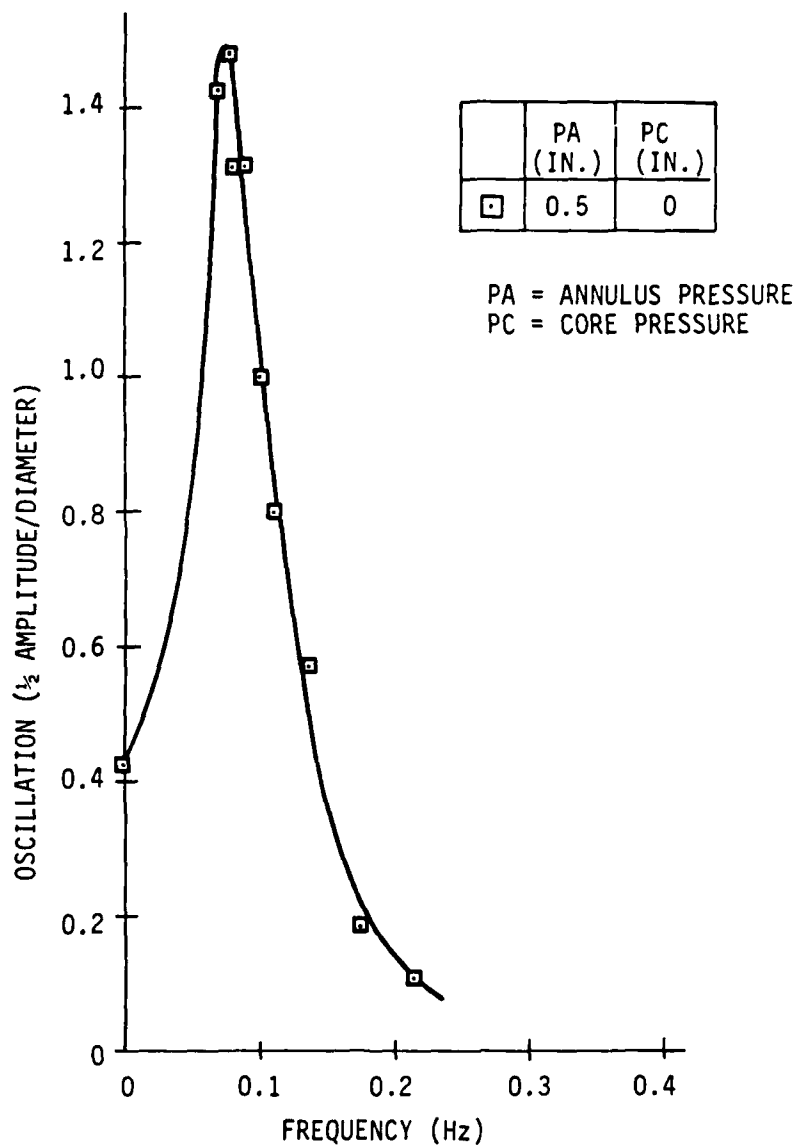


Figure 19 VARIATION OF PIPE OSCILLATION WITH FORCING FREQUENCY, RUN 11 (BALLAST WEIGHT, 13 LB)

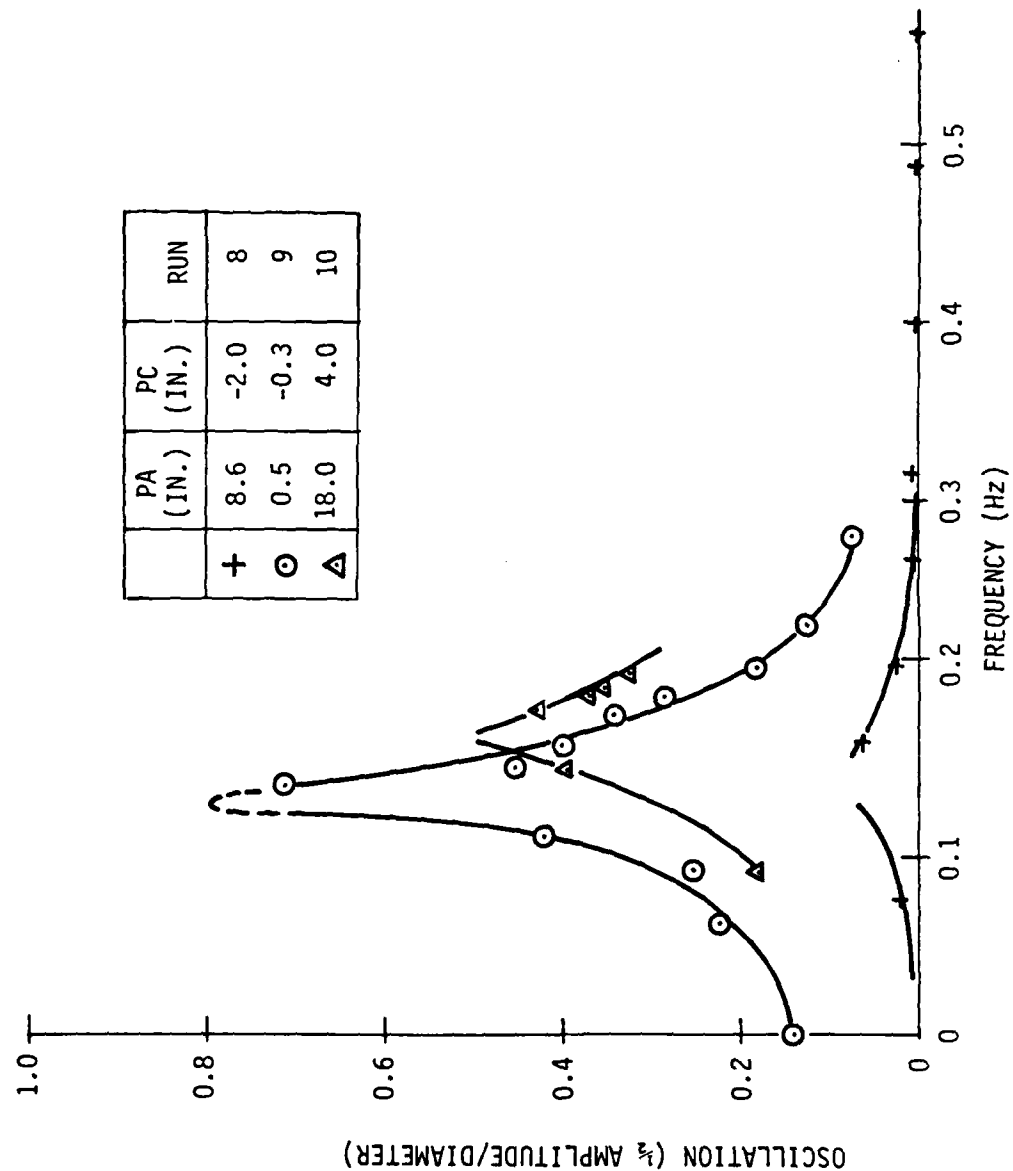


Figure 20 VARIATION OF PIPE OSCILLATION WITH FORCING FREQUENCY, RUNS 8, 9, AND 10  
(BALLAST WEIGHT, 36.05 LB)

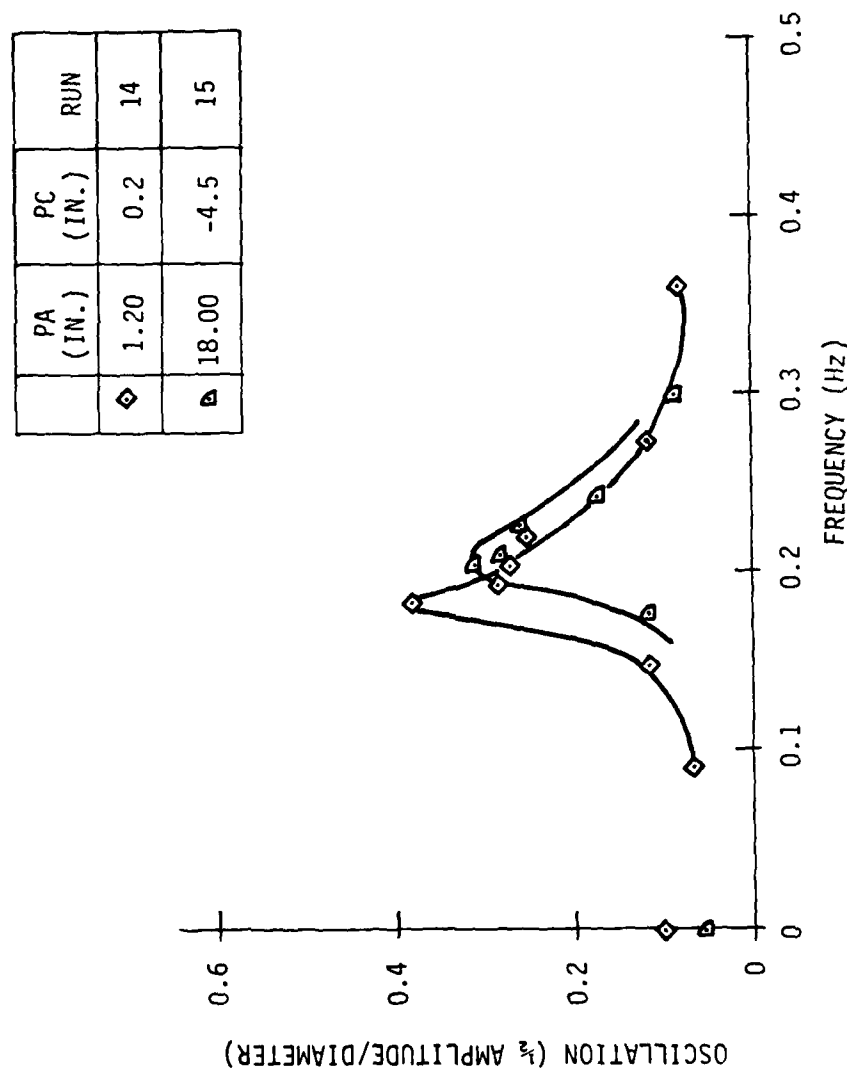


Figure 21 VARIATION OF PIPE OSCILLATION WITH FORCING FREQUENCY,  
RUNS 14 AND 15 (BALLAST WEIGHT, .83 LB)

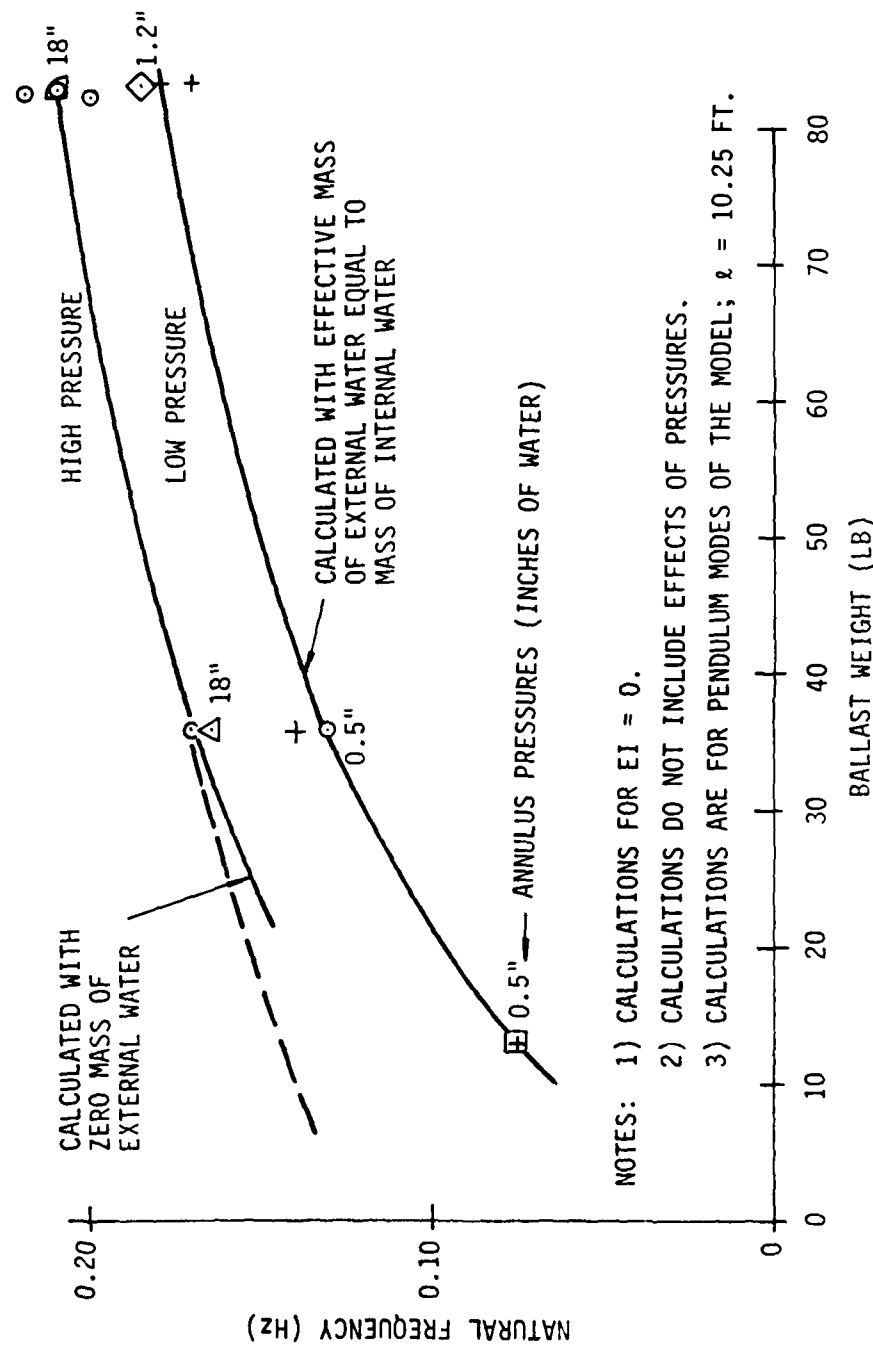


Figure 22 VARIATION OF NATURAL FREQUENCY WITH BALLAST

Figure 22 shows the effects of ballast weight and annulus pressure on the pendulum-mode natural frequencies. In general, the model was observed to vibrate in the pendulum mode. Although the model was cantilevered from the metal header pipe (the standpipe was clamped to the support frame), lateral deflections did not have the characteristic first-mode shape of a beam. Instead, it acted more as a rigid member with a pivot just below the pipe attachment to the metal header pipe. This is confirmed by records from the three accelerometers taken at the model CWP upper, middle, and lower sections (table VII). For some of the higher forcing frequencies, there appeared to be some indication of a very slight pipe bending about a point near its attachment to the header pipe.

When lateral-motion amplitudes at the bottom of the pipe were large (about  $\pm 0.5$  to  $\pm 1$  diameter or more), buckles developed just below the header pipe. These occurred twice per cycle, on the sides of the pipe that were compressed by the lateral oscillations.

Efforts to excite a second mode of vibration were generally unsuccessful; however, a few visual indications of a second mode were observed. These permitted estimates of a second-mode frequency near 0.7 and 0.9 Hz with 36- and 83-pound ballast weights, respectively.

TABLE VII

## COMPARISON OF DATA FROM UPPER, MIDDLE, AND LOWER ACCELEROMETERS\*

RUN NUMBER	SCALE READING OF DEFLECTION			FREQUENCY (Hz)	TEST PHASE
	BOTTOM	MIDDLE	TOP		
9-5	5.0	5.6	4.8	0.141	Vibration
10-4	3.2	3.4	3.0	0.184	
11-9	5.0	5.2	4.2	0.076	
14-4	2.6	3.2	3.0	0.185	
15-3	2.2	2.8	2.6	0.205	
16-15	8.2	8.0	7.8	0.071	Tow
17-7	4.7/3.6	4.8/4.0	3.8/3.0	0.175	
19-4	6.0/3.5	5.8/3.4	4.8/2.8	0.118	
20-10	4.2/3.5	4.0	5.0	0.208	
21-4	8.2/3.6	8.0/4.2	7.2/3.0	0.172	Tow

\*Data taken at peak values.

Figure 23 is a summary plot of the peak response amplitudes from the response-versus-frequency plots of tests at various ballast weight and pressure combinations. Despite the large ranges of ballast weight and annulus pressure, all points fall on a single curve. The effect of the corrections for  $\theta$  and  $\delta$  contributions to the accelerometer outputs are shown by the corrected  $\delta_T/D$  curve. The dashed line indicates that the peak  $\delta_T/D$  decrease versus frequency is not quite proportional to  $(1/f)^2$ . By inspection, it appears that this decrease lies between a  $1/f$  and  $(1/f)^2$  trend.

The pendulum-mode damping, with the model in the water, was estimated from decaying oscillations occurring when the waterjets were turned off. If the small restoring moment at the header due to the model bending stiffness is neglected, a pendulum-mode motion equation can be written as:

$$I\ddot{\theta} + R\dot{\theta} + W_B L\theta = 0$$

where

$W_B$  = Ballast weight corrected for buoyancy

$R$  = A linear damping coefficient [used for mathematical convenience; actual damping is mostly hydrodynamic damping proportional to  $(\dot{\theta})^2$ ]

$\theta$  = Angular deflection relative to vertical (radians)

$\dot{\theta}$  = Angular velocity (rad/sec)

$\ddot{\theta}$  = Angular acceleration (rad/sec/sec).

The effect of bending stiffness could be accounted for by a slightly higher factor in place of  $W_B L$ .

If the waterjets are shut off, the envelope of the decaying oscillations is then theoretically defined by:

$$\theta(t) = \theta_0 e^{-Ct}$$

where

$\theta_0$  = Initial amplitude

$e$  = Base for natural logarithms (2.718)

$C$  =  $R/2I$ , the logarithmic decrement

$t$  = Time.

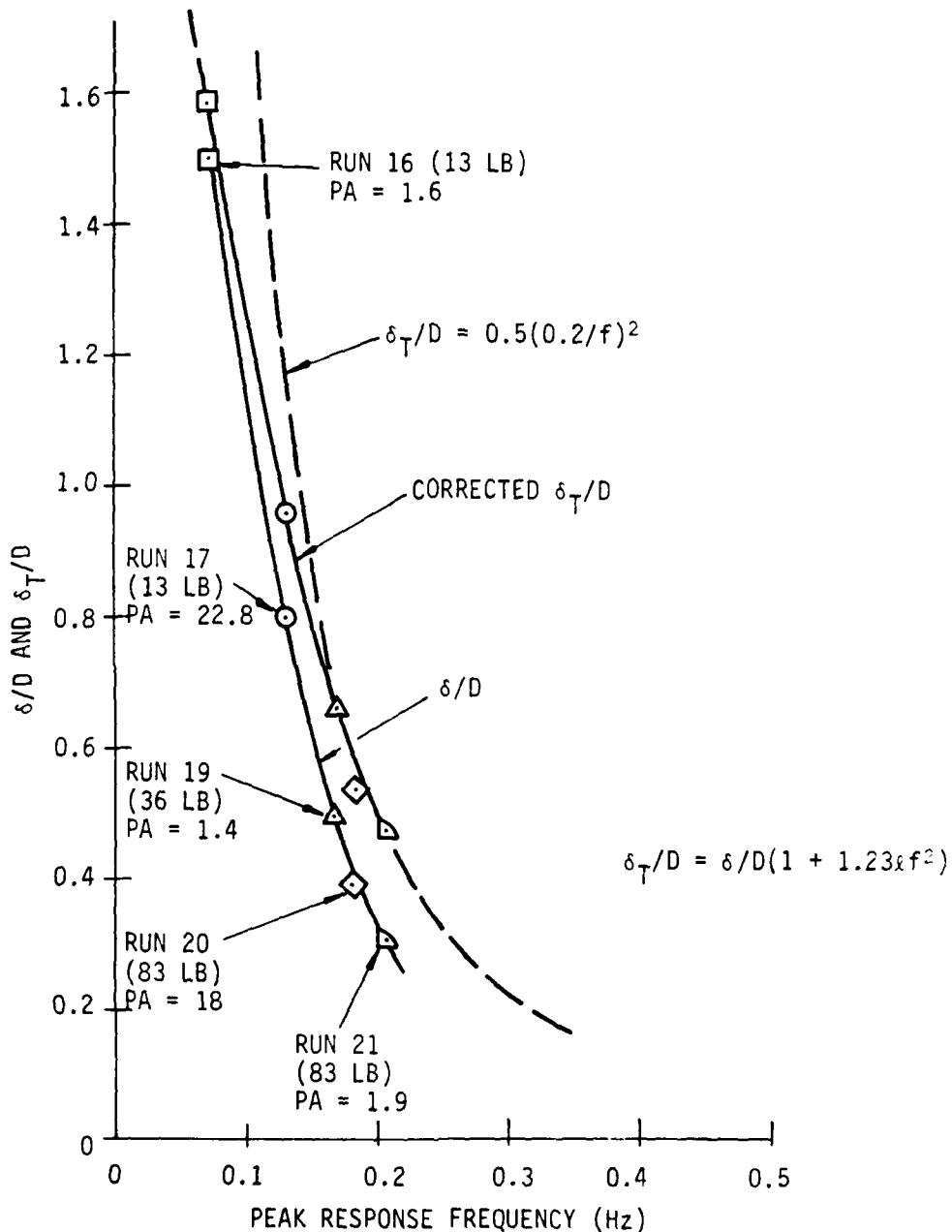


Figure 23 VIBRATION TEST PEAK RESPONSE AMPLITUDE  
VERSUS PEAK RESPONSE FREQUENCY

The pendulum natural frequency with damping is given by

$$\omega_n = \sqrt{\frac{W_B L}{I} - \frac{R^2}{4I^2}} \quad (\text{rad/sec})$$

and

$$f_n = \frac{\omega_n}{2\pi} \quad (\text{Hz})$$

where  $\omega_n$  = vibration velocity (rad/sec) and  $f_n$  = frequency (Hz).

If  $R/2I$  is small relative to  $W_B L/I$ , the frequency from the oscillograph records is an adequate approximation of  $f_n$  or  $\omega_n$ . If

$$\frac{R}{2I} = \sqrt{\frac{W_B L}{I}}$$

equals the undamped natural frequency, the initial displacement will decay exponentially without oscillations. The damping value that results in this situation is the critical damping. The ratio

$$(R/R_{\text{critical}}) = \frac{R/2I}{\sqrt{\frac{W_B L}{I}}}$$

is the damping ratio. If  $(R/R_{\text{critical}})$  is approximately 0.3 or less,

$$(R/R_{\text{critical}}) \approx \frac{R/2I}{2\pi f_n}$$

where the approximation results from the use of  $f_n$  (the damped natural frequency from the oscillogram of decaying oscillations) instead of the undamped frequency. This decay frequency ( $f_n$ ) should be the same as the frequency which produced maximum response in the vibration test.

Figure 24 is an example of oscillations decaying after the waterjets were turned off. The logarithmic decrement for this case was computed to be -0.15; the corresponding damping is approximately 28 percent of critical damping. The frequency of the decaying oscillations is 0.086 Hz. This is slightly higher than

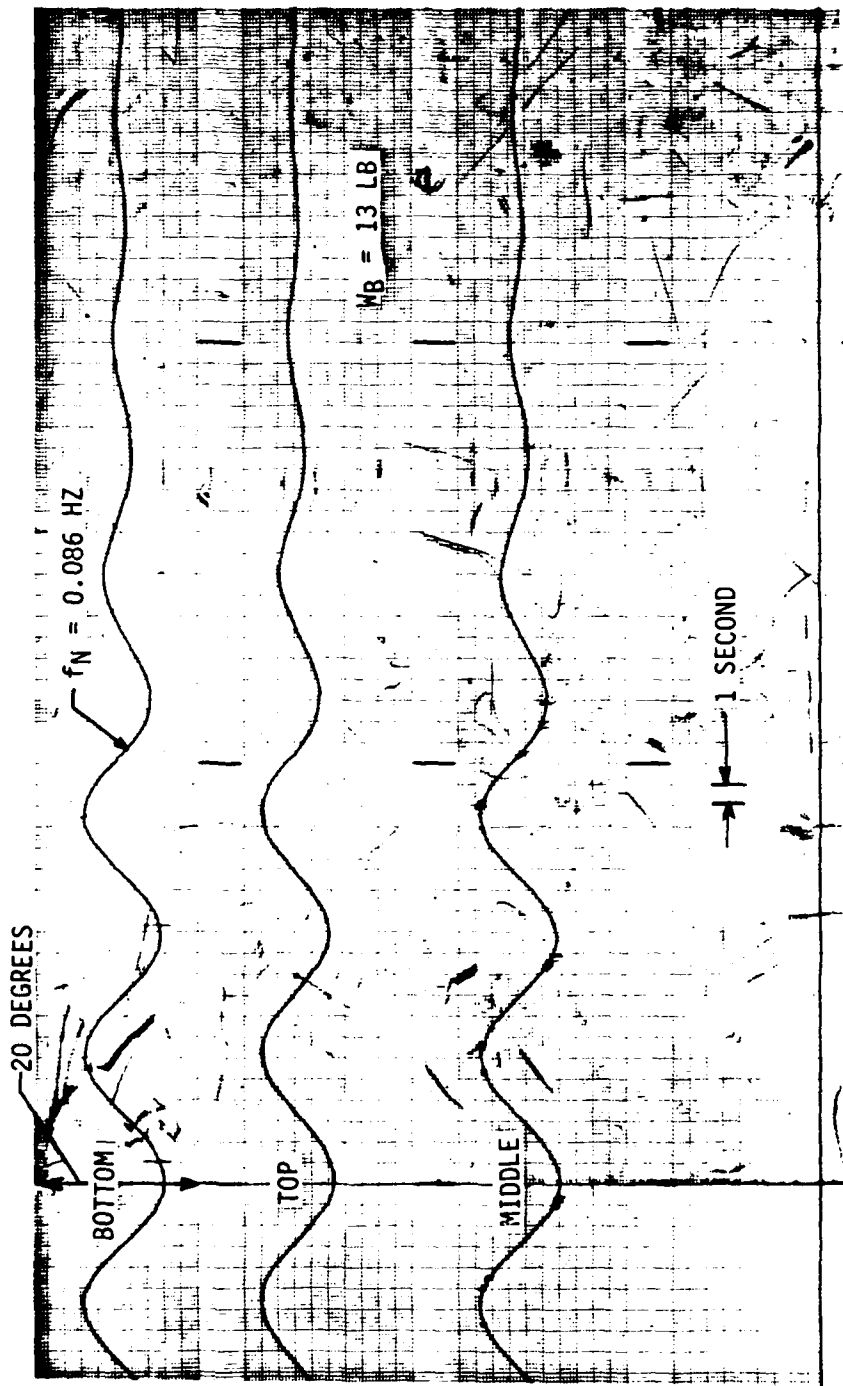


Figure 24 DECAYING OSCILLATION: RUN 11-10

the natural frequency determined from the response curve peak in figure 19. This difference may be attributed to experimental error in definition of the figure 19 peak, and/or nonlinear frequency-versus-amplitude effects.

### 8.3 Tow Tests

The variation of pipe lateral oscillatory displacement and frequency with forward speed is shown in figures 25 through 29 for the three ballast-weight conditions tested. Figures 25 and 26 give the results for the 13-pound-ballast-weight condition at low- and high-pressure levels. It can be seen that the peak oscillation for the low-pressure condition occurs at a frequency of 0.075 Hz, which was the natural frequency measured for this condition in the earlier vibration tests (figure 19).

Figure 27 shows the results for the 36-pound-ballast condition at low-pressure levels. Again, the peak amplitude appears to be at about the natural frequency. The results for high and low pressure at the 83-pound-ballast condition are given in figures 28 and 29. The peak displacements for these two conditions, and the velocities which produce maximum displacement, are not as clearly defined as for the other cases. However, the frequencies at maximum amplitudes are near the natural frequencies measured earlier.

Figure 30 summarizes the effects of ballast weight and annulus pressure on peak response frequency during the tow tests. It is very similar to figure 22 for the vibration tests. Small differences between the two figures are probably due to uncertainties in the peak response frequencies and small pressure differences, rather than an actual difference between vibration and tow test characteristics.

Figure 31 summarizes peak response magnitudes from the tow tests. Trends are very similar to those from the vibration tests in figure 23. The one exception is the data from run 21. Other than motion amplitudes, there were no fundamental differences between motion characteristics from run 21 and the other runs in this figure. Data system gains were kept the same for the bottom accelerometer (used for this figure) during all tests; therefore, the differences are not due to a data error.

A comparison of figure 28 (high pressure) with figure 29 (low pressure) suggests that maximum possible amplitudes might not have developed during the figure 28 test at a velocity of 1.0 ft/sec. If the amplitude response for this one run were doubled, the shape of the figure 28 response curve would be similar to figure 29, and the point for run 20 on figure 31 would be as indicated by the dashed symbol. The trend versus frequency for the 83-pound-ballast cases would then be similar to the trend indicated by the other runs.

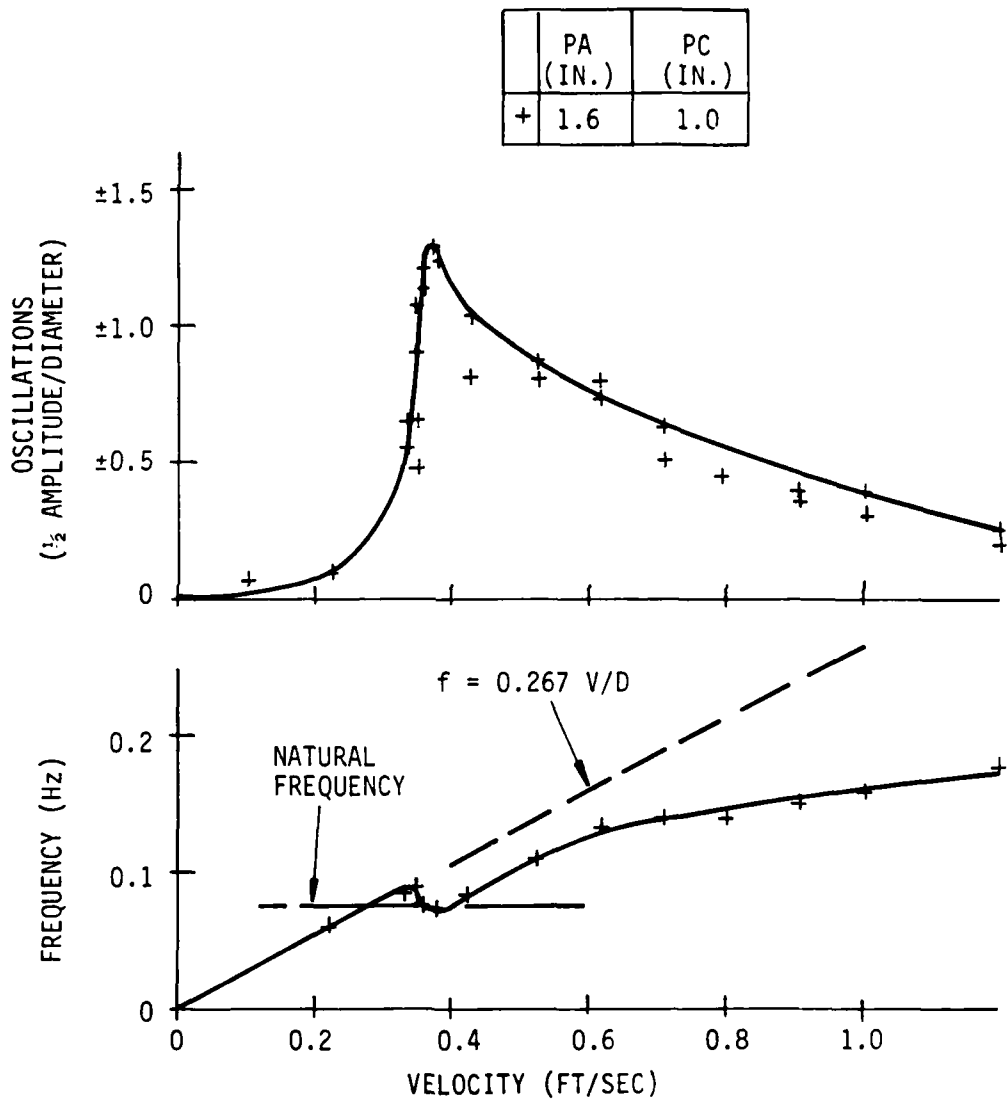


Figure 25 VARIATION OF PIPE LATERAL DISPLACEMENT AND FREQUENCY WITH SPEED, RUN 16 (BALLAST WEIGHT, 13 LB)

	PA (IN.)	PC (IN.)
○	22.8	-4.0

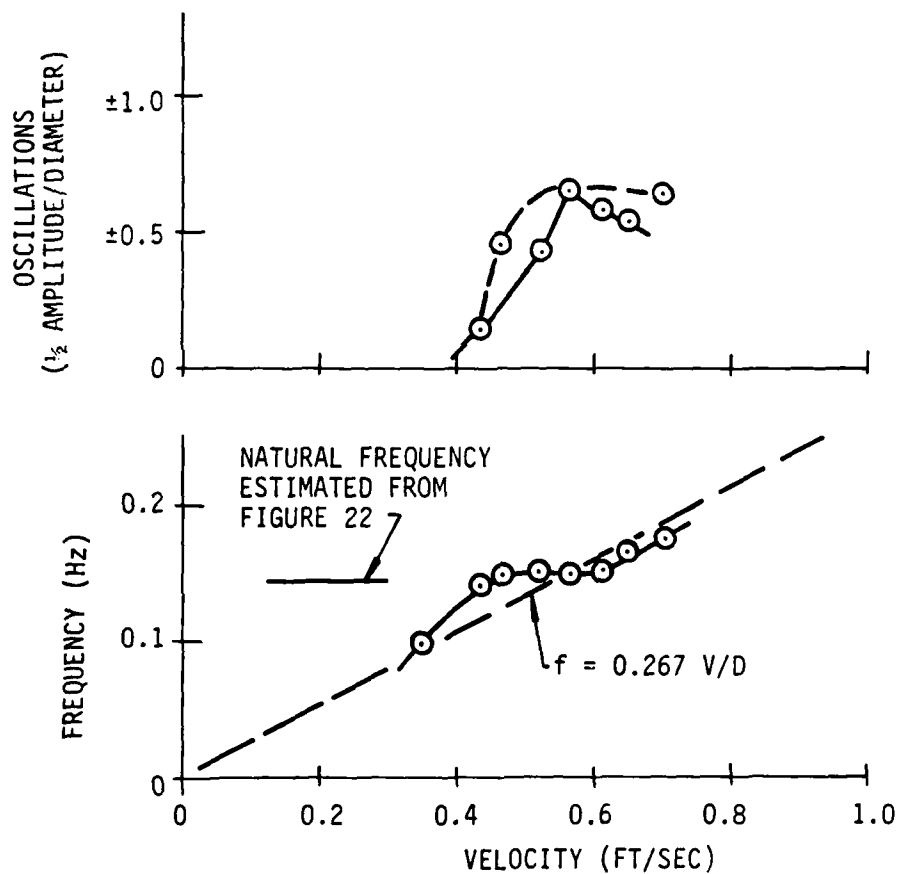


Figure 26 VARIATION OF PIPE LATERAL DISPLACEMENT AND FREQUENCY WITH SPEED, RUN 17 (BALLAST WEIGHT, 13 LB)

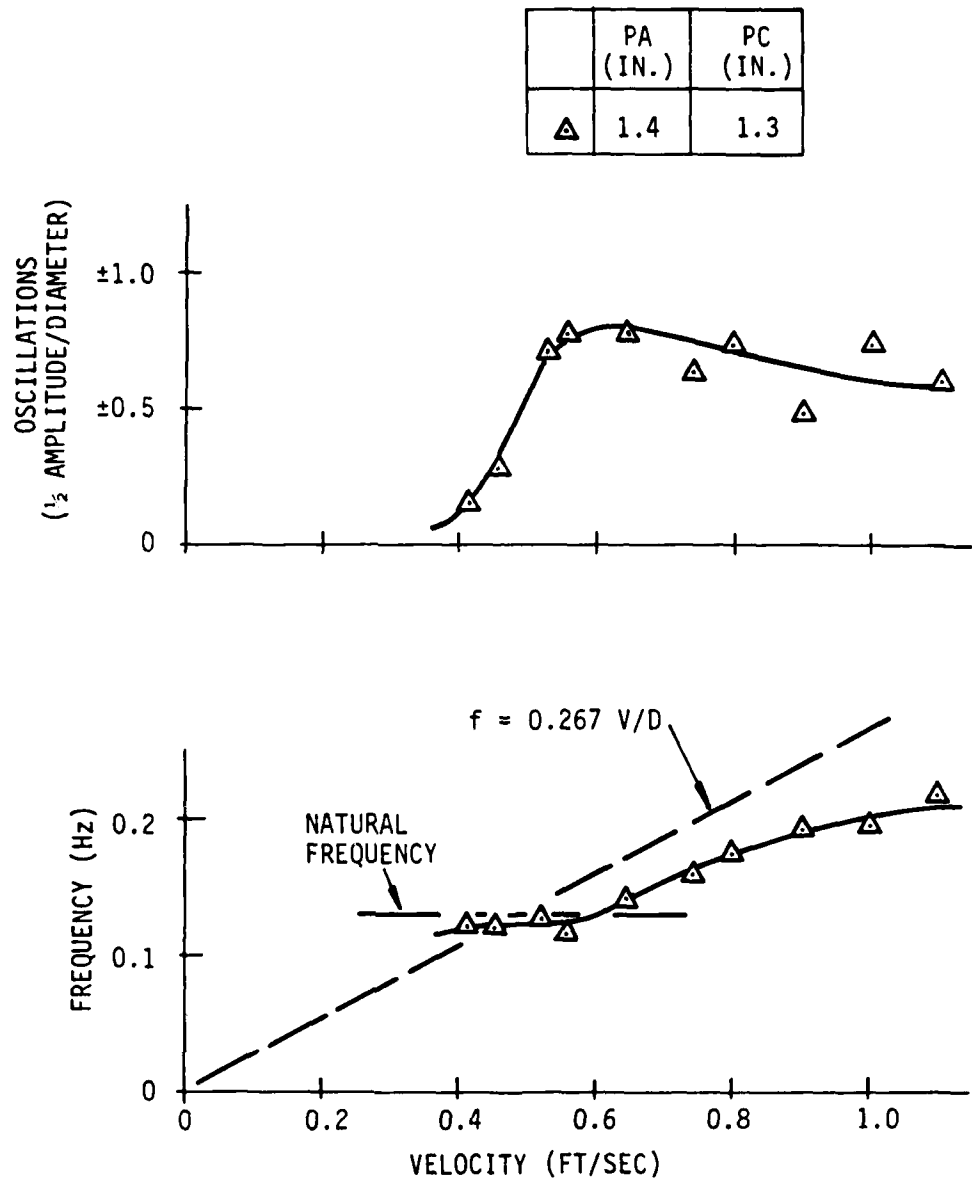


Figure 27 VARIATION OF PIPE LATERAL DISPLACEMENT AND FREQUENCY WITH SPEED, RUN 19 (BALLAST WEIGHT, 36 LB)

	PA (IN.)	PC (IN.)
◆	18.0	-4.0

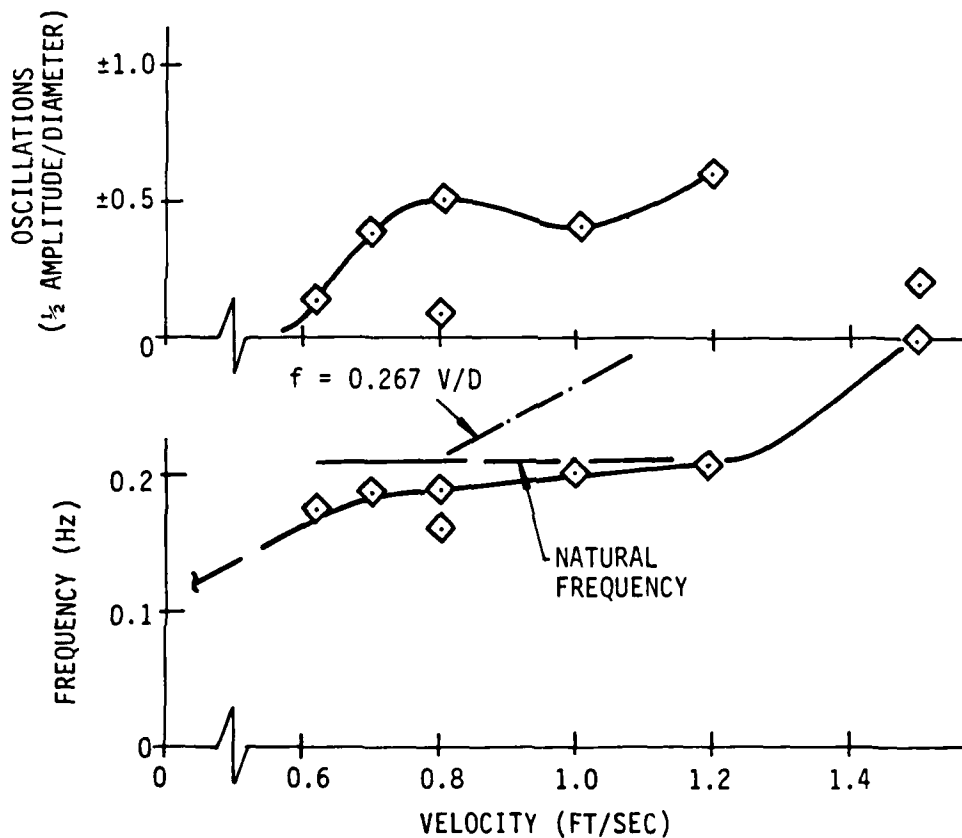


Figure 28 VARIATION OF PIPE LATERAL DISPLACEMENT AND FREQUENCY WITH SPEED, RUN 20 (BALLAST WEIGHT, 83 LB)

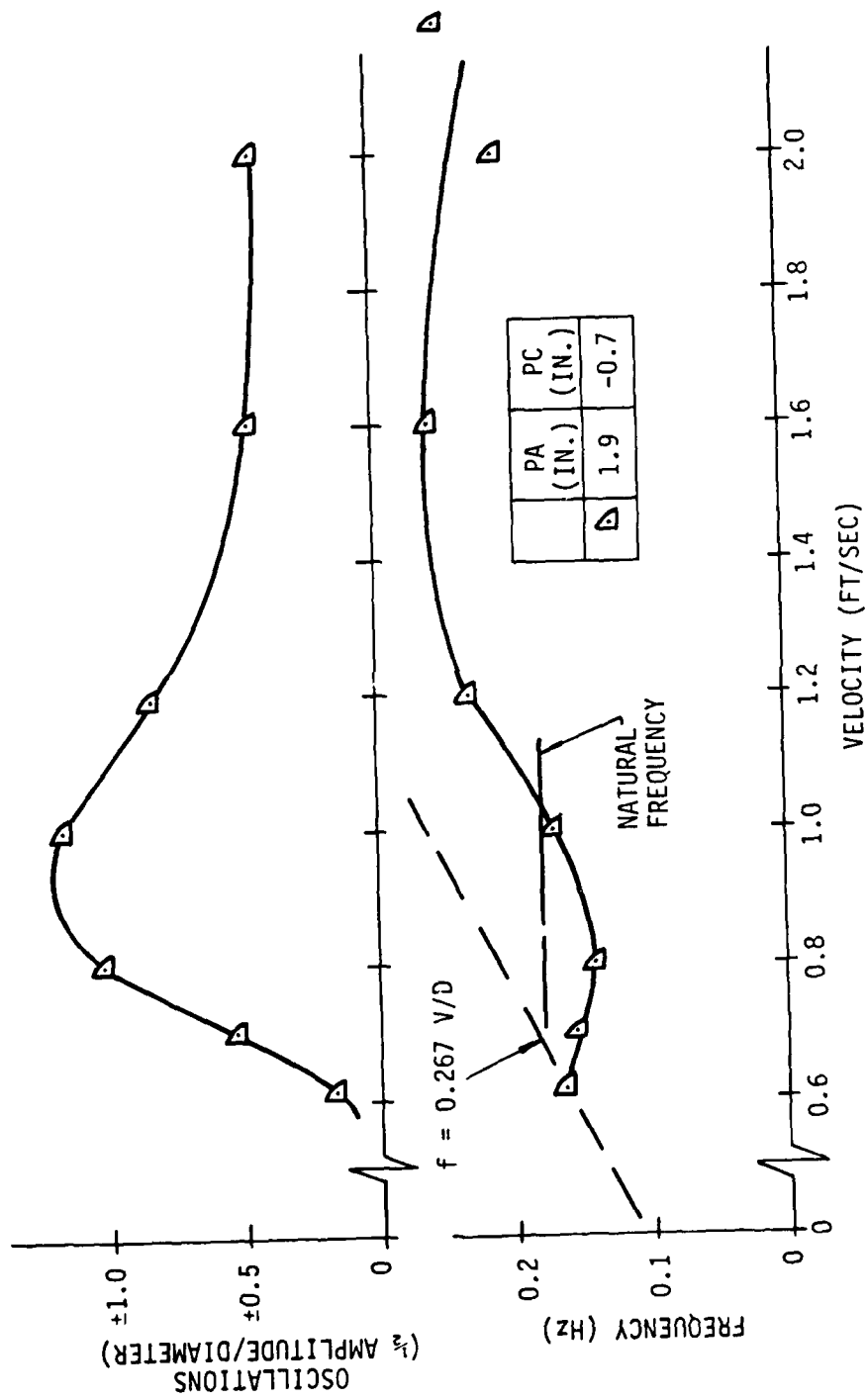


Figure 29 VARIATION OF PIPE LATERAL DISPLACEMENT AND FREQUENCY  
WITH SPEED, RUN 21 (BALLAST WEIGHT, 83 LB)

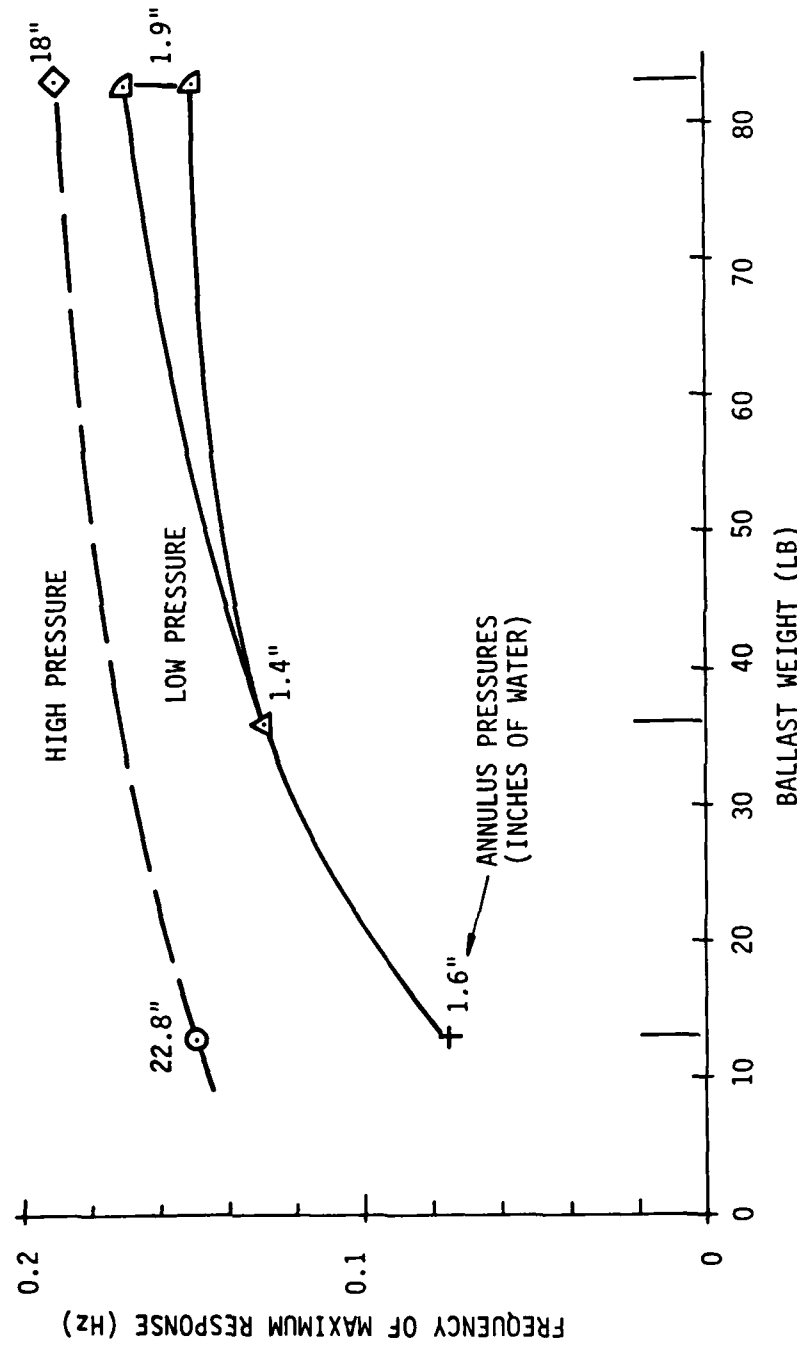


Figure 30 FREQUENCY OF PEAK RESPONSE VERSUS  
BALLAST WEIGHT DURING TOW TESTS

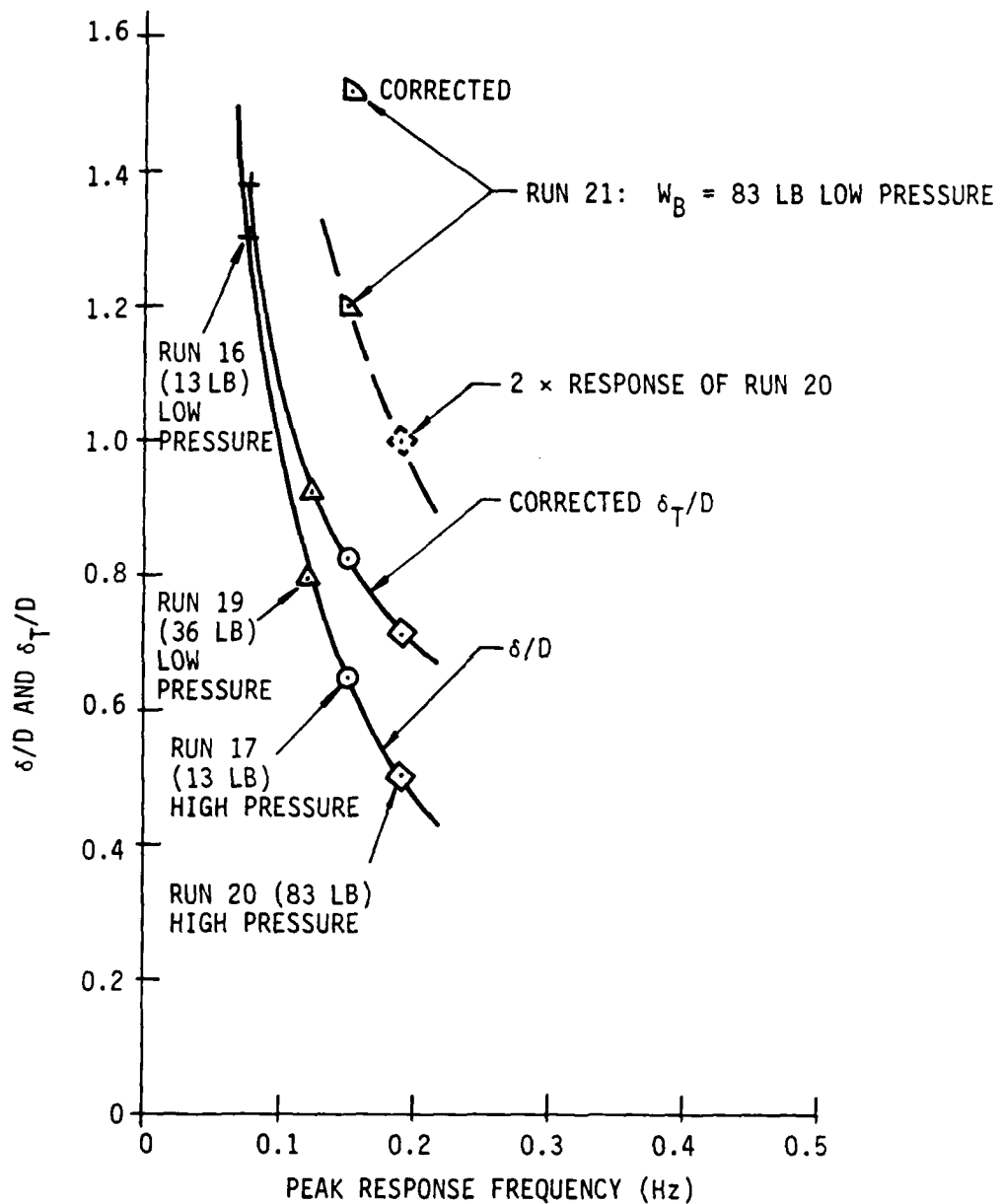


Figure 31 TOW TEST PEAK RESPONSE AMPLITUDE  
VERSUS PEAK RESPONSE FREQUENCY

It is also possible that additional or longer runs might have increased the peak response magnitudes for runs 16, 17, and 19 (figures 25, 26, 27). Most runs were continued until oscillations had stabilized. For cases where long-term amplitude variations were evident, runs were extended through at least one growth and decrease cycle. Stable amplitudes, or evidence of long-term variations, were generally observed within five oscillations. Most runs were for at least 20 cycles. The run 20 test, at 1 ft/sec, was a case where the run was terminated after 10 cycles because oscillations were very steady.

It is speculated that nonlinear effects of material characteristics, or buckles, may have contributed to the difference between run 21 and most other runs. This and/or deflection changes due to drag with oscillation amplitudes may have contributed to small frequency changes that affected the degree of tuning and, hence, the amplitudes. Run 21 was one of the series of tests in which the long-term growth and decay of oscillations was very evident. This was also evident in many of the other of tests 16 through 21, but to a lesser degree than for run 21. During most of the series 24 runs, the minimum oscillation amplitudes were about 1/3 to 1/2 of the maximums plotted on figure 29.

In general, the model vibrated in the pendulum mode at the lower tow speeds and lower ballast conditions tested. However, with the higher ballasts it was possible to test at higher speeds where a second-mode vibration was transiently excited.

It was noted from oscillograph records that at some speeds there was a long-term increase and decrease in the CWP pendulum-mode amplitude; this can be seen in the sample record, figures 32, 33, and 34. The drag deflections also had a long-term increase and decrease that correlated with vibration amplitudes. This indicates a drag increase when the pipe oscillations were large.

When lateral vibration amplitudes were large, buckles occurred twice per oscillation, and were located on the compression sides at the attachment to the header pipe. Such buckles either would not occur, or would be less severe, on more elastic full-scale CWPs with higher L/Ds and greater axial elongations due to ballast and pressure.

Small buckles also occurred on the model leading side when drag deflections were equivalent to several diameters. These buckles occurred near the mid-depth point on the model, which is the point of maximum bending moment with the header pipe free to pivot aft. Also, the buckling occurred at approximately the predicted velocities, which were in excess of scaled velocities for full-scale pipes. Corresponding drag deflections were one to two diameters, depending on the ballast weight.

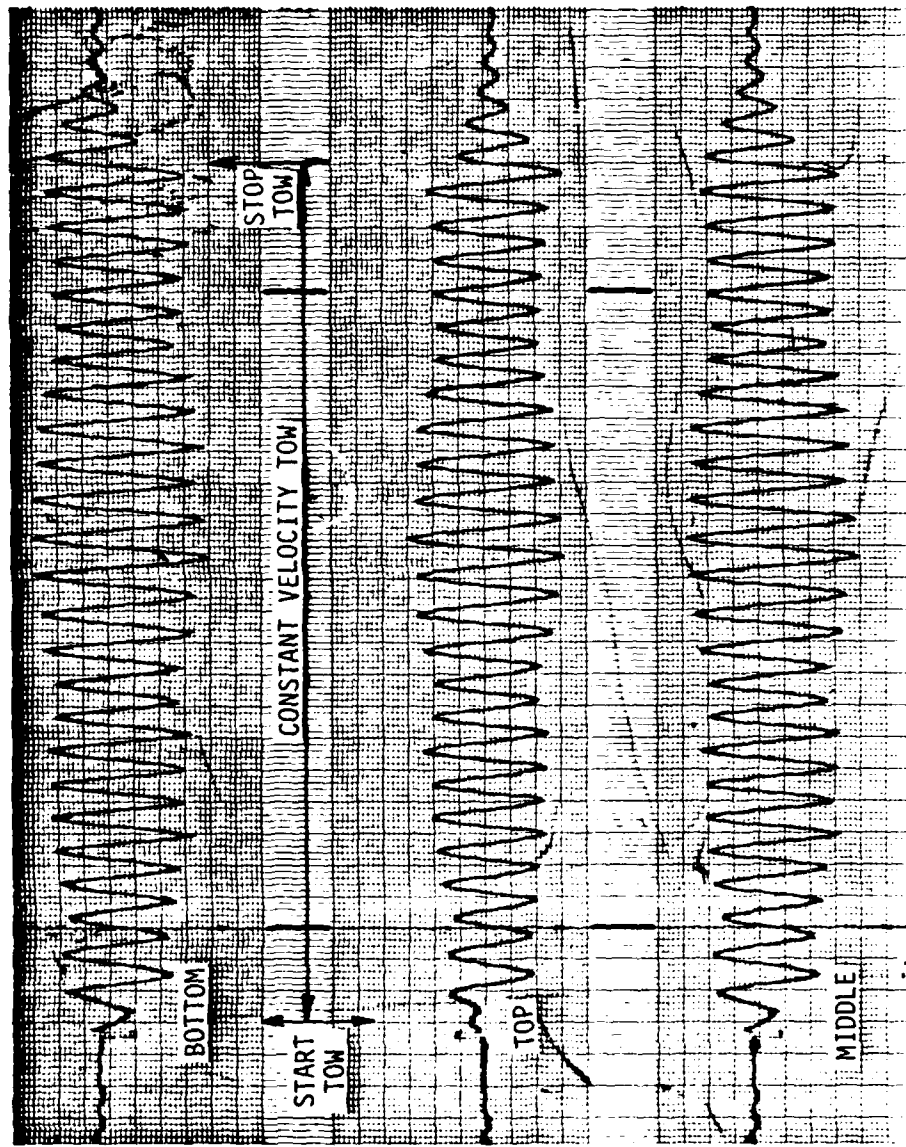


Figure 32 AMPLITUDE VARIATIONS DURING CONSTANT VELOCITY TOW

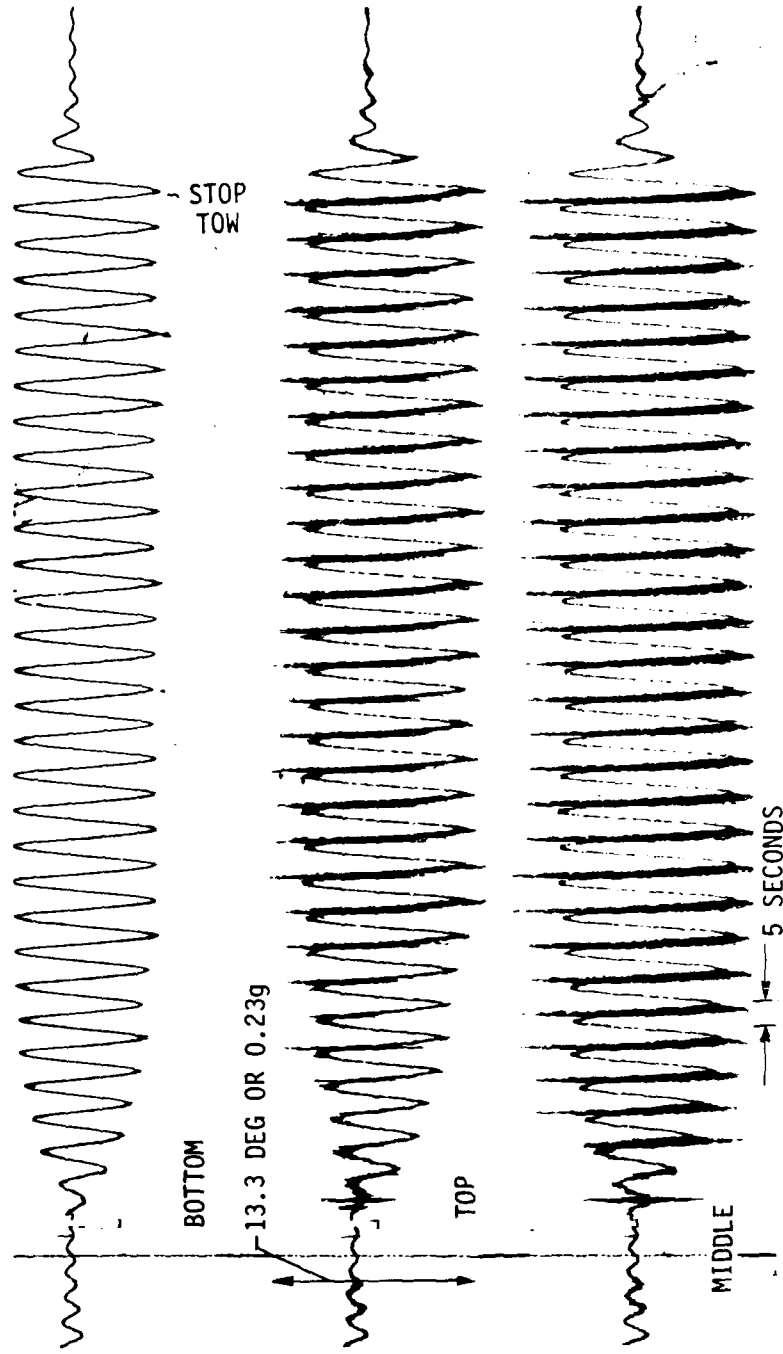


Figure 33 HIGH-FREQUENCY OSCILLATIONS, RUN 21-3, TOW VELOCITY = 0.805 FT/SEC

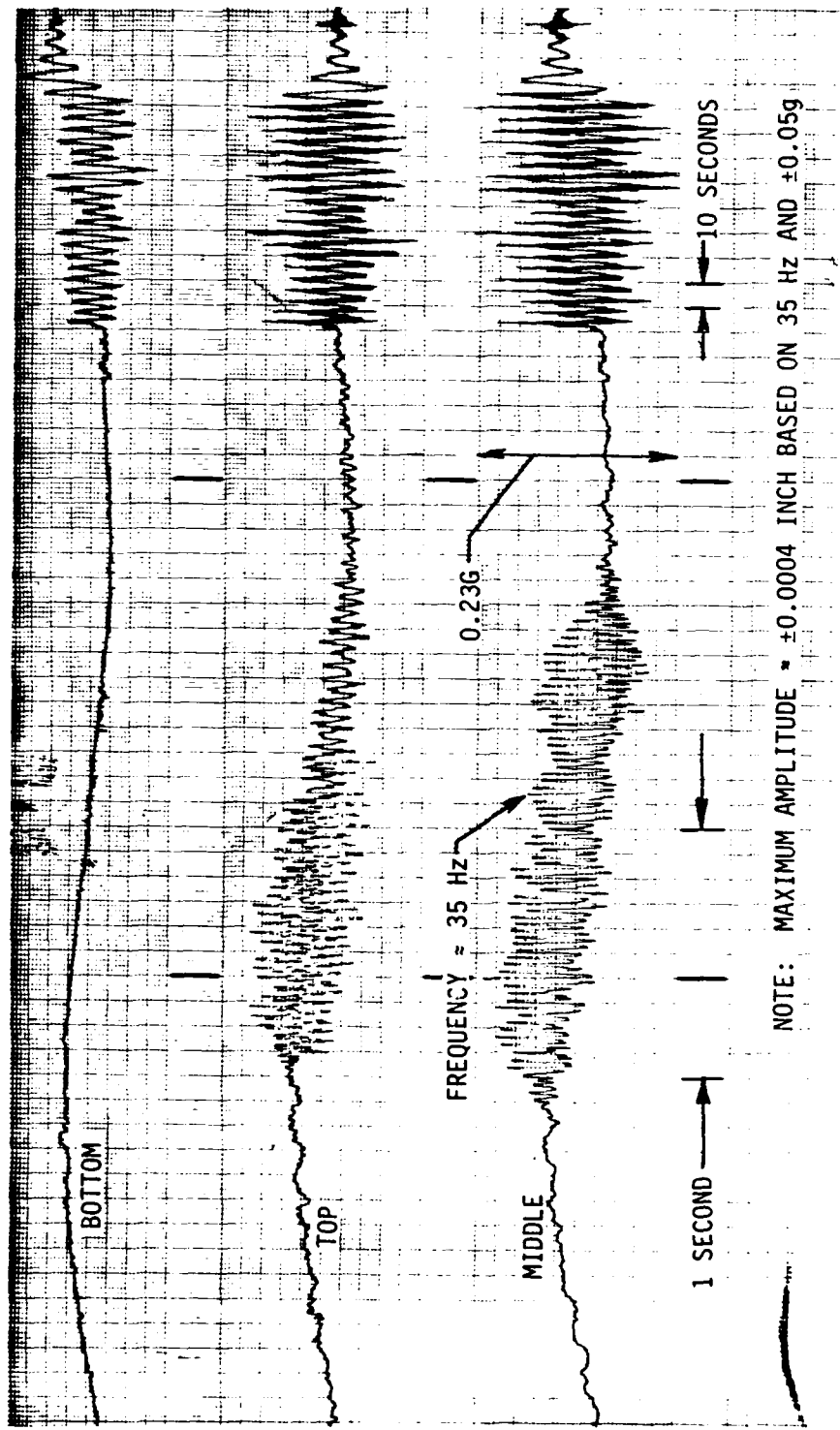


Figure 34 HIGH-FREQUENCY OSCILLATIONS AT EXPANDED TIME SCALE,  
RUN 19-8, TOW VELOCITY = 1.1 FT/SEC

Figure 35 shows the local slopes of the model and the lateral deflections obtained by integrating these slopes. The slopes were obtained from table VII by applying the static calibration factors; these were then corrected for frequency effects to obtain plot two. The bottom portion of figure 35 shows the lateral deflection obtained by assuming a rigid-body rotation and using data from the bottom accelerometer without the frequency correction. Also shown is the deflected shape derived from all three accelerometers with the frequency correction. Although differences are not negligible, they would not affect general conclusions drawn from other plots in this report that are based on the bottom accelerometer without the frequency correction.

Figure 36 shows the aft deflection variation of the ballast can bottom with towing speed, for most of the conditions tested. At higher speeds, the ballast can was dragged beneath the carriage; thus, deflection measurements could not be obtained. It would appear that the deflections were not proportional to velocity squared, as would be the case with a rigid body in steady-flow conditions. It was observed during the tests that, in addition to the long-term lateral-oscillation amplitude changes of the pipe, there was an unsteady long-term deflection change in the drag direction. Drag deflections, plotted in figure 36, are the maximum deflections that occurred when oscillations were largest. Although the model CWP did have freedom to pivot aft, the mass of the header pipe below the pivot did provide some resistance to pipe deflection. Rough estimates, based on figure 36 data, indicate the pipe had an effective or average drag coefficient that ranged from about 0.8 to 2.2. The higher values were obtained from times when oscillations were large. Because these are only preliminary estimates, further analysis of drag data is recommended.

During the course of the tests, a check was made of the flow patterns around the model. Polystyrene dust was spread over the water surface and the model towed through it. The flow was observed around the cylindrical header pipe, and with the model raised so that the lobes pierced the free surface. The presence of shedding vortices was noted, with no apparent difference between the patterns around the cylindrical header pipe and those around the lobed flexible pipe. Figure 37 is a photograph of the flow pattern around the flexible pipe. In addition, spoilers were attached to the smooth-walled ballast container to check if this was a major contributor to the vortex shedding. Figure 38 shows the location of the spoilers. No significant effect was measured, as can be seen from run 18 in figure 36.

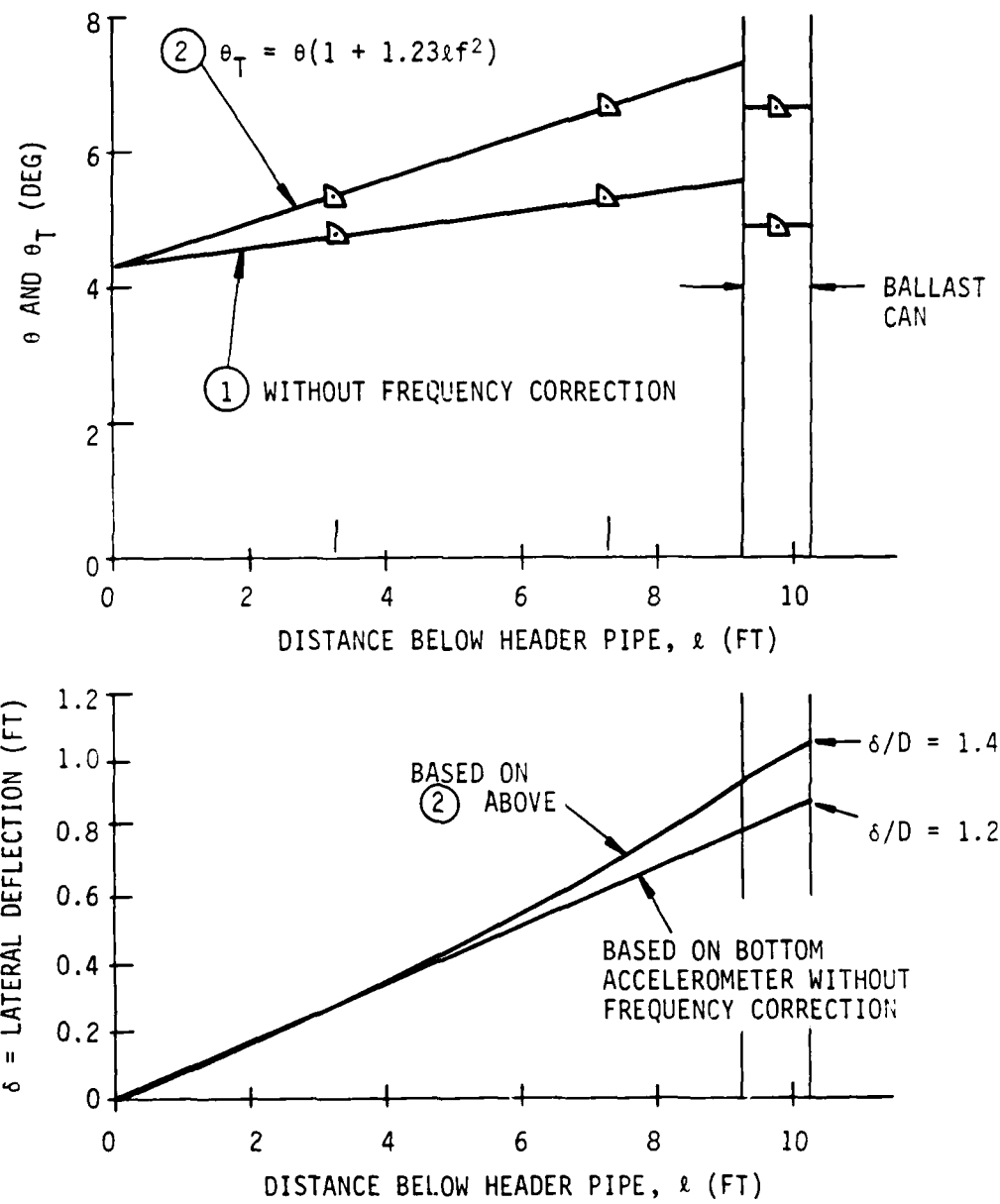


Figure 35 EXAMPLE OF PENDULUM-MODE SHAPE,  
TOW RUN 21-4,  $f = 0.172$  Hz

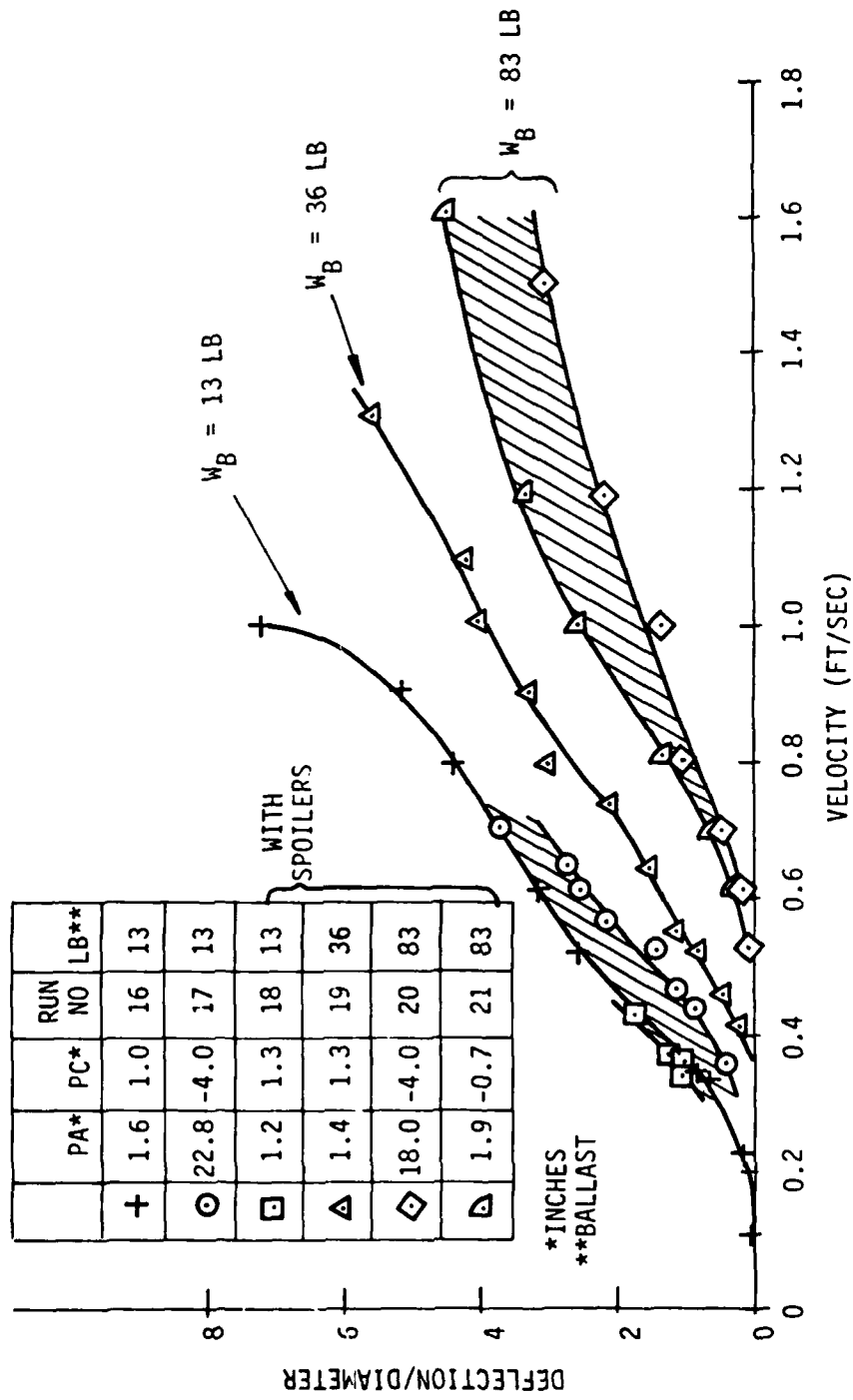


Figure 36 VARIATION OF PIPE DEFLECTION (AFT) WITH SPEED

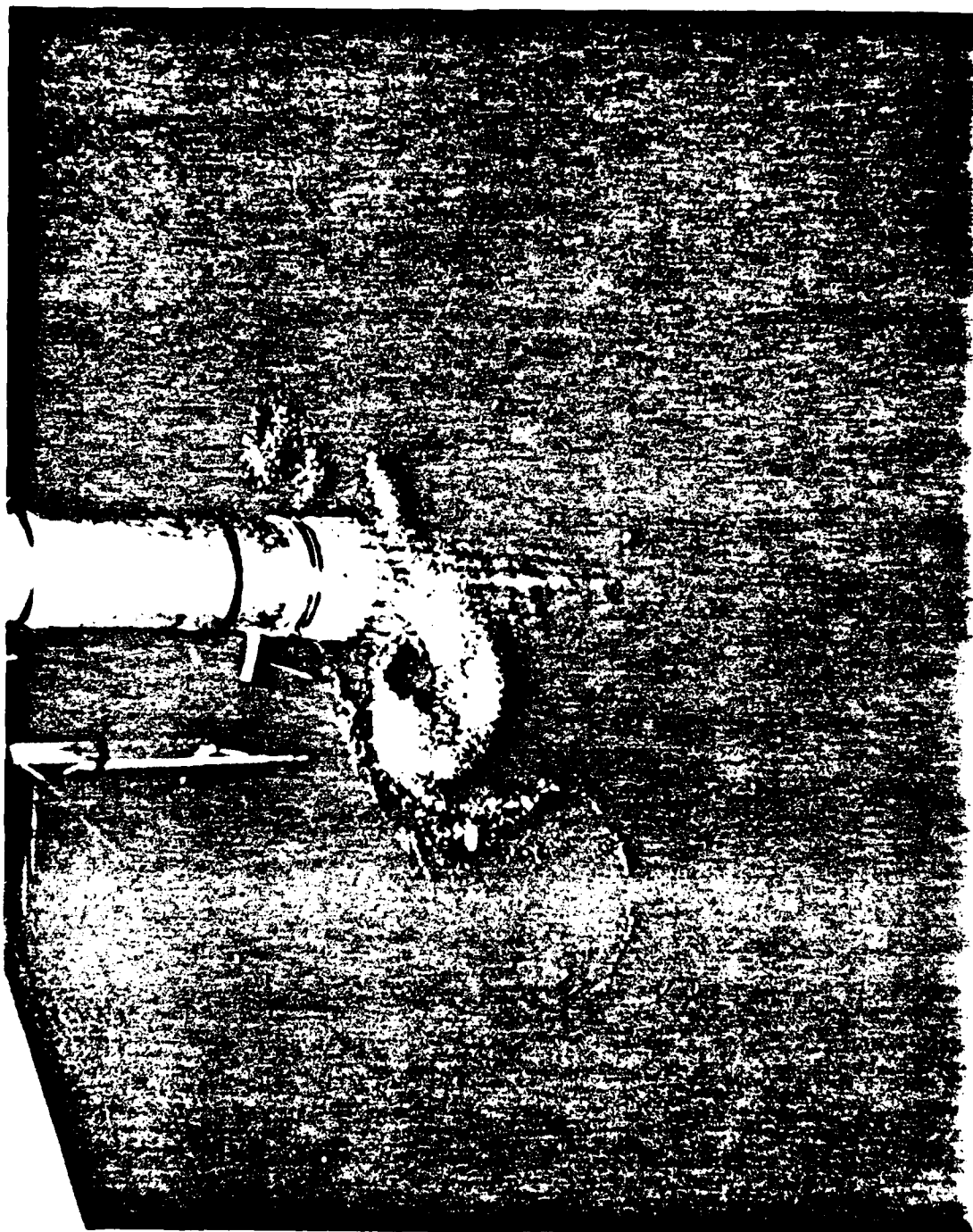


Figure 37 PHOTOGRAPH OF FLOW PATTERN AROUND MODEL CWP

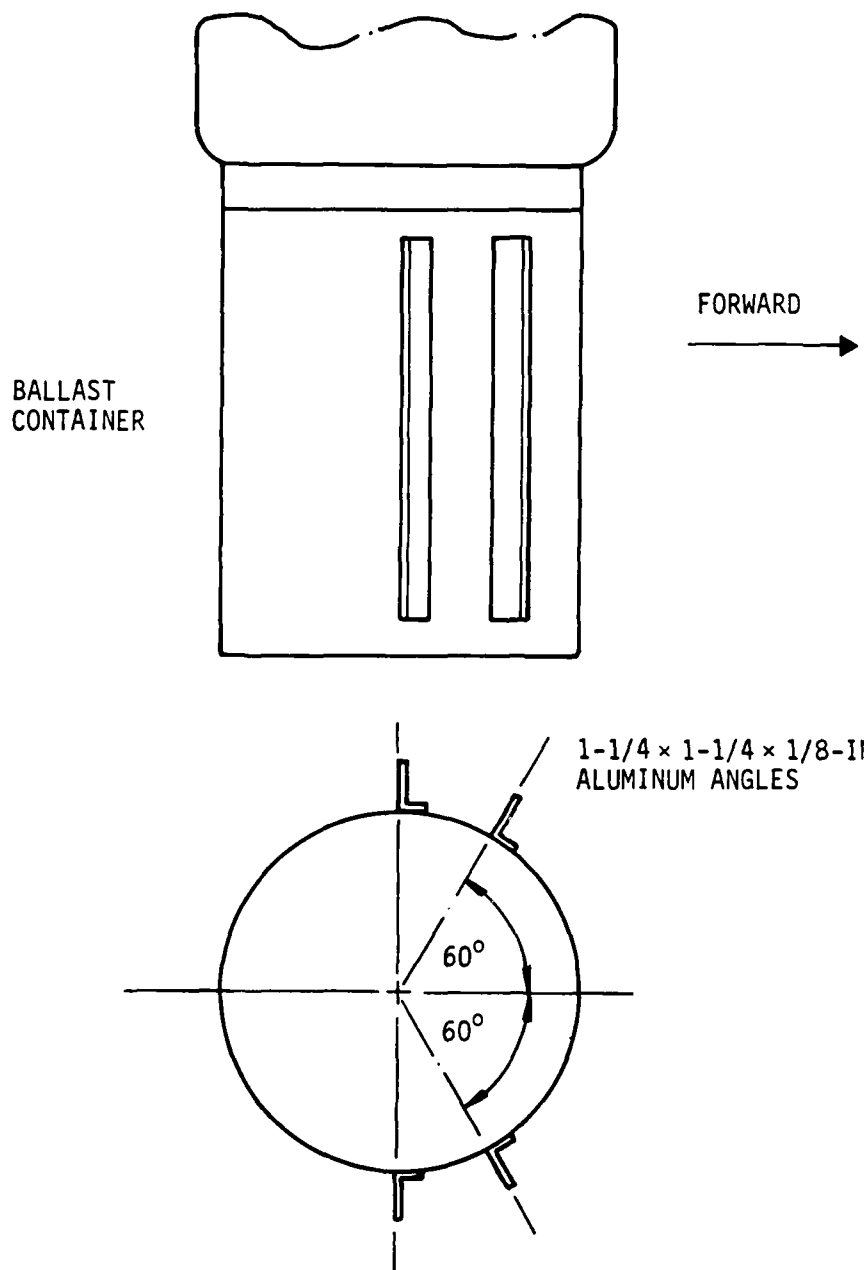


Figure 38 LOCATION OF SPOILERS

## 9. INTERPRETATION OF RESULTS

### 9.1 Static Ring Buckling Tests

Bell uses a digital computer program that will solve force-balance equations for a two-dimensional (2D) double-walled flexible pipe to optimize geometries, pressures, etc., for OTEC pipes. The nonlinear load-versus-elongation characteristics of materials can be used in this program. A subroutine calculates an effective EI of a section through the annulus, and uses a buckling equation for cylinders to calculate the annulus pressure required for cross-section stability when the pipe internal pressure is reduced.

The model tests showed that this method, in its present form, is unconservative. However, the required annulus pressure increase implied by the test results does not result in a large increase in material strength or weight. This is because, for concepts which Bell has explored, material weight has been influenced more by ballast weight than by annulus pressure, and because material weight does not increase in proportion to strength (coating thickness can be kept relatively constant as fabric strength is increased).

The static buckle tests indicated that existing force-balance equations (which assume a circular cross section) should be extended to permit solutions for cases where the section deviates from circular. Such solutions should predict required annulus pressures that are consistent with the model test results. After this has been verified, the modified equations can be used to study effects of cross-section geometry on required annulus pressure.

Although the equations now available for buckling pressure predictions were found to be unconservative, basic mechanics of the cross-section buckling suggests that the equations should be valid for estimates of the effects of material characteristics on buckling pressures. Computer runs with model and full-scale stiffnesses, varied by a factor of 5, resulted in insignificant changes in predicted buckling pressures. This was expected because in typical full-scale pipes, nominal material elongations are about 10 percent or less. Model nominal elongations were less than 2 percent. The changes in elongation, from just before to just after section buckling, are much less than this 2 percent. The primary changes at the buckle boundary are changes of the directions and magnitudes of the forces which must balance at each node or cross-section junction. These directions and magnitudes are insensitive to material elasticity, and the forces are functions of annulus pressure divided by core pressure, for a given cross section.

As demonstrated by the model CWP tests, the annulus-pressure-to-core-pressure ratio at the buckle boundary is, for all practical purposes, a constant for a given cross-section geometry (figures 4 and 6). If effects of material elongation characteristics (especially nonlinearities) were significant, this ratio would vary as a function of the pressures. Both basic mechanics and

the test results show that the pressure ratio, at the buckle boundary, is very insensitive to material elongation characteristics. Therefore, the static buckle test results (annulus pressure/core pressure) can be applied directly to full-scale pipes with geometrically similar cross sections.

Further studies should be made, with modified equations, to investigate effects of cross-section geometry on buckle boundaries, to develop designs with improved buckle characteristics, and to reoptimize designs for full-scale flexible CWPs.

## 9.2 Vibration Tests

Vibration tests defined response-versus-frequency curves for several ballast weight and pressure combinations (figures 19 through 21).

### 9.2.1 Vibration Amplitudes

Figure 23 shows that the amplitudes of maximum responses decrease with increases of ballast weight and/or pressure. Simple analyses, equating energy input per cycle to energy dissipated per cycle, indicated that peak amplitudes for these tests could be expected to decrease in proportion to  $(f_n)^2$ , where  $f_n$  is the natural frequency (frequency of maximum response) for each configuration tested. This relationship would be expected to be exact if energy dissipation were due entirely to hydrodynamic dissipation forces that are proportional to  $\dot{Y}^2$ , where  $\dot{Y}$  is the local lateral velocity of the pipe due to vibratory motion.

If the peak amplitude of 1.5 diameters at 0.07 Hz from figure 23 is proportioned down in relation to  $(f_n)^2$ , one would predict an amplitude of 0.40 diameters when  $f_n$  is 0.135 Hz, and 0.17 diameters when  $f_n$  is 0.21 Hz. The peaks in figures 20 and 21 are higher than the amplitudes calculated by the proportioning. This suggests that either the energy dissipation due to vibratory motions of the model CWP through the water is not proportional to the square of vibratory velocity, or there is significant damping due to pipe material or internal water, which is not proportioned to  $\dot{Y}^2$ .

Vibration tests with the model in air would be required to separate external and internal energy dissipation factors. Vibration tests with the model CWP filled with water cannot be conducted in air because the head of water would overpressurize the model. Tests of the model in air while pressurized with air might not be representative because energy would not be dissipated by internal water, and because natural frequencies would be too high without the mass of the internal water. Analyses with parametric variations of external damping functions might be used to match trends from the test and, hence, infer appropriate dissipation functions.

Because of the lower than desired model L/D and the higher than desired model CWP bending stiffness, the vibration tests cannot be directly applied to full-scale pipes. The results can be used to verify or improve analytical methods of predicting flexible pipe modes, frequencies, and damping. They also provide insight into what factors must be considered in analyses of full-scale pipes.

#### **9.2.2 Ballast Effects**

Because the model was not a true scale model of a full-scale pipe, emphasis in the vibration tests was on determining trends versus ballast weight and pressures over ranges greater than those representative of typical scale values. Figure 22 indicates that even though the model EI in bending was too high, the calculations using  $EI = 0$  predicted frequencies of the first mode that were of the correct order of magnitude, and the measured trends versus ballast weight were similar to predictions. The model vibration characteristics were analyzed only in an approximate manner using calculations for limiting cases to help establish the model design and test plans. The predictions in figure 22 assumed that in the first mode the model acted like a pendulum rotating about its attachment to the metal support. Observations, TV pictures, and accelerometer data showed that in this mode, the model behaved as a rigid pendulum, with very little bending along its length.

#### **9.2.3 Effective Water Mass**

The predictions in figure 22 are for two different assumptions concerning the effective mass of water external to the pipe core and annulus. They assume that the water in the core and annulus has an inertia; but, because the model and this water are neutrally buoyant, the only restoring force is that due to gravity acting on the ballast weight. The effective ballast weight is reduced slightly by buoyancy forces. Curves are shown for an effective inertia of external water being zero, and an effective inertia of external water equaling the inertia of the internal water.

The fact that data points lie near the zero effective mass of external water curve does not prove that the effective mass of external water was low. The calculated lines on this figure assumed the model EI was zero. Calculated EI was approximately 22,000 lb-in<sup>2</sup>. This would raise the test frequencies relative to the calculated curves.

#### **9.2.4 Pressure Effects**

The data points on figure 22 show an increase of natural frequencies with an increase in pressures. Because the tests covered large pressure differences, the test pressure effects were large compared to what could be expected for practical pressure changes in full-scale pipes. The pressure effects shown in figure 22 are believed due to higher pressures placing the nominal or working loads in the model fabric at higher load points on the

load-versus-elongation curve. The material-load-versus-elongation curve slope is higher at higher loads than at very low loads. This results in a larger EI, or bending stiffness, at the higher pressures.

#### 9.2.5 Vibration Modes

Prior to the tests, it was hoped that it would be possible to excite a second, and possibly even a third, mode of vibration. Analyses, treating the pipe as a string ( $EI = 0$ ) with the ballast producing a string tension, showed a trend of natural frequencies versus ballast weight very similar to the trends in figure 22. With a ballast weight of 83 pounds (the maximum used in the tests), the frequencies of the first two string modes were estimated to be less than 0.4 to 0.8 Hz.

Estimates treating the model as a beam with zero ballast, and neglecting gravity effects, indicated that first and second bending modes would exist at a frequency near 0.1 and 0.5 Hz when the ballast was very small. Efforts to excite a second mode with the waterjets on the ballast can were not very successful. While there appeared to be a second mode with a frequency near 0.7 Hz with a 36-pound ballast, and between 0.9 and 1.0 Hz with an 83-pound ballast, the measured accelerations were too low and wave forms too irregular to define a response curve or mode shapes. However, the visual observations and TV pictures indicated mode shapes similar to that in figure 39. This is the general shape expected for a second mode. The limited second-mode shape and frequency data indicates that if a computer program were used, with both EI stiffness effects and tension forces due to gravity acting on the ballast, it would probably give reasonable estimates of at least the first two or three frequencies and mode shapes of the model.

The figure 39 mode shape suggests that attempts to excite the second mode probably would have been more successful if the waterjets had been relocated to a point about halfway up the model. The excitation forces are most effective in exciting a vibration mode if the forces are applied at a maximum-amplitude point of a given mode shape. Time constraints prevented such tests.

#### 9.2.6 Extrapolation to Full Scale

Frequency equations for a string, and for a beam, suggest that because of the short model length, EI effects on the modes and frequencies of the model CWP were more significant than they would be for full-scale pipes.

For a string (with ballast much less than weight of water in the pipe),

$$f_n = \frac{2n - 1}{4L} \sqrt{\frac{T}{u}} \quad (\text{if the bottom can translate}),$$

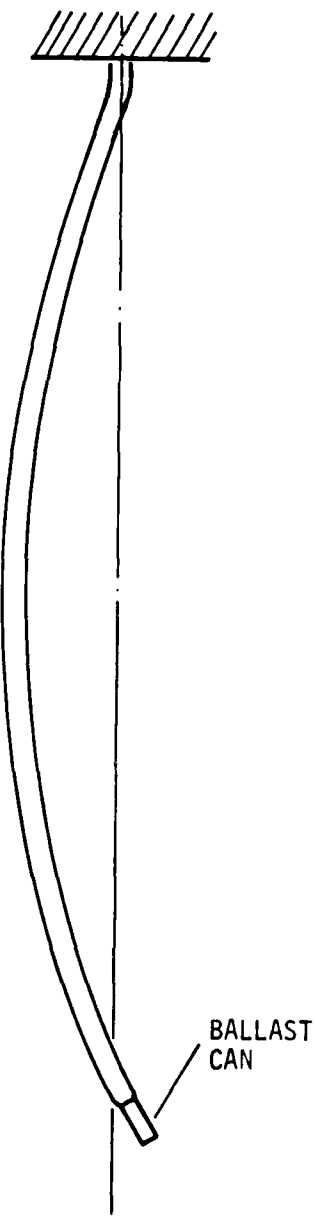


**Figure 39 SKETCH OF OBSERVED  
SECOND-MODE SHAPE**

or

$$f_n = \frac{2n}{4L} \sqrt{\frac{T}{u}} \quad (\text{if the bottom is pinned}).$$

For a uniform beam (without tip weight),

$$f_n = \frac{a_n}{2\pi L^2} \sqrt{\frac{EI}{u}}$$

where

$a_n = 3.52, 22.4, 61.7, \text{ etc,}$  and is constant in the beam frequency equation.

The combined effects of  $L^2$  in the beam equation versus  $L$  in the string equation, and the more rapid increase of  $a_n$  versus  $n$  relative to increases of  $2n - 1$  and  $2n$ , caused EI to have a greater effect on frequencies of the model than it would on a higher L/D model. On actual pipes, with much higher L/Ds, the EI effects should be small, except possibly for very high modes. Vibration tests of a higher L/D model would be desirable to verify this and to validate computer programs which include EI and tensile effects.

The above approximate equations might be used to extrapolate model first- and second-mode frequencies to full-scale pipes, by proportioning test frequencies based on ratios of length, EIs, tension due to ballast, etc. However, the value of such extrapolations is questionable because these simple equations do not account for combined EI and tension, or gravity, effects.

A better approach appears to be the validity verification of existing computer programs based on these tests, or tests of longer models, and the use of computer programs to calculate full-scale CWP frequencies.

The most important result of the vibration tests was that there were no surprises or unexpected results. Also, the tests indicated that use of pulsed waterjets is a feasible method of exciting flexible pipe vibration modes with the pipe immersed in water.

### 9.3 Tow Tests

#### 9.3.1 First-Mode Vibration

The tow test results were generally as expected. The first mode of vibration (pendulum mode) was excited by vortex shedding when the tow velocity was increased to the point where the vortex-shedding frequency matched the natural frequency of the model. The slopes of frequency versus velocity lines from

the origins to the flat spots of tow-test frequency-response curves (figures 25 through 29) indicate a Strohal number of approximately 0.27. This is reasonable for these tests with low Reynolds numbers.

### 9.3.2 Higher Modes

In general, attempts to further increase the tow velocity to excite the second mode were unsuccessful, because drag deflections became very large before the vortex frequency matched the second-mode frequency. This resulted in reductions of velocities normal to upper portions of the pipe, plus buckles and complex three-dimensional (3D) shapes (due to drag plus lateral oscillations), which probably made the system very nonlinear.

There were a few observations of transient second-mode motions with the largest ballast weight, indicating that this mode was excited at tow velocities of 2 to 2.5 ft/sec (table VI).

Based on the well defined excitation of the first mode at about 0.9 ft/sec (figure 29), for a case when the model had a first-mode frequency near 0.2 Hz (figure 21), excitation of a second mode (with a frequency of 0.7 to 1.0 Hz) was expected at a velocity of 3 to 4.5 ft/sec. Based on tests up to 2.5 ft/sec, drag deflections would have resulted in a nearly horizontal pipe position before these velocities were reached.

### 9.3.3 Frequency and Drag Relations

Approximate equations for pipe natural frequencies (section 9.2.6), and the vortex-shedding-frequency equation ( $f_v = S \cdot V/D$ ), can be used to solve for the velocity where the vortex-shedding frequency matches a pipe natural frequency. Then, using simplified calculations for the drag deflection, the following equations can be derived.

For cantilever or beam modes (with small ballast weights),

$$\frac{\delta_D}{OD} = \frac{Cd(a_n)^2}{8\pi(2\pi)^2 (144 SN^2)} .$$

For string modes,

$$\frac{\delta_D}{OD} = \frac{Cd(2n - 1)^2}{32\pi SN^2} \text{ or } \frac{CD(2n)^2}{32\pi SN^2}$$

where

$\delta_D$  = Deflection of pipe bottom due to drag when nth mode is excited by vortex shedding

OD = Outside diameter

SN = Strouhal number

Cd = Drag coefficient.

If the pipe were pinned so that it could rotate aft due to drag, as it was during these tests, there would be a different constant in the beam-mode equation.

The interesting aspect of these equations is that they are independent of diameter, model length, or ballast weight. This suggests that a similar situation would exist if calculations of pipe frequencies and drag deflections were made with combined EI and tension effects.

The implication is that for a given model configuration (ballast weight and pressure), if the first mode was excited when  $\delta_D/OD$  was about one (see figure 36 and figures 25 through 29), the first mode of a full-scale pipe would also be excited when  $\delta_D/OD = 1$ . This would be true even though the full-scale pipe had a much higher L/OD. If Reynolds number effects change the ratio of Cd/SN<sup>2</sup>, then the full-scale  $\delta_D/OD$  would be affected by the change in this ratio.

The string mode  $\delta_D/OD$  equations suggest that the second mode would be excited when the  $\delta_D/OD$  was  $(2n-1)^2 = 9$  to  $(4)^2 = 16$  times the  $\delta_D/OD$ , which existed when the first mode was excited. The beam equation suggests the  $\delta_D/OD$  ratio would be  $(22.4/3.52)^2 = 40$  if EI effects dominated tension effects on deflections and frequencies. Therefore, it is not surprising that second modes were not excited before drag deflections became unrealistically large.

#### 9.3.4 Higher-Mode Test Methods

The preceding relationships assume a constant current along the length of the pipe, as in a tow tank. The above discussion indicates that even if a high L/D model could be tested, drag deflections in a uniform current are likely to become large before velocities are high enough to excite a second mode. They are almost certain to become excessive before a third mode is excited. This is consistent with what was experienced during these model tests.

This discussion also suggests that if tests are to be made to measure higher-lateral-mode responses of very flexible pipes, it will either be necessary to simulate currents which decrease with depth (to reduce drag deflections,

while high current velocities near the surface excite higher modes), or the bottom of the model must be constrained against drag and uniform velocity tests must be used to validate analyses rather than to directly simulate full-scale pipes.

#### 9.3.5 Extrapolation to Full Scale

The model CWP peak-response amplitudes during tow tests were comparable to those during the vibration tests. Again there was a trend of decreased amplitudes with ballast weight and pressure increases. The largest response was approximately  $\pm 1.3$  diameters. This was relatively large for the low L/D model. Maximum motions of full-scale pipes would be expected to be less than  $\pm 1.5$  diameters because of effects of the nonuniform currents versus depths. Reference 1 indicates that maximum amplitudes can be expected to be less than 2 diameters. This is consistent with these test results. However, motions considerably greater than 2 diameters would not create significant stresses in high L/D full-scale pipes. The periods of the pendulum modes of such full-scale pipes would be measured in minutes rather than seconds.

#### 9.3.6 Local Oscillations

In addition to the excitation of first lateral-vibration modes, and some transient excitation of a second mode, there were some indications of local oscillations of pipe material, illustrated in figure 33. A high-frequency noise is evident from the two accelerometers on the fabric, but not from the accelerometer on the ballast can. The oscillations occurred only during one-half cycle of the pipe lateral motions, when the motion direction was such that the accelerometers were on the leading side of the model.

Figure 34 is a playback showing these local oscillations at a very-high paper speed. Wave forms are irregular, but frequencies were about 35 Hz. Based on these frequencies and corresponding accelerations of approximately  $\pm 0.05g$ , motion amplitudes were approximately  $\pm 0.0004$  inch. Although visibility was reasonably good down to the level of the upper accelerometer, these very small oscillations could not be seen.

At this time, it is believed that these oscillations are probably not representative of what can be expected on full-scale pipes. Although each accelerometer only weighed 4 grams, this is still a large weight compared to the weight of a very local area of fabric ( $0.057 \text{ gr/in}^2$ ) that was probably oscillating. It could also be significant relative to a very small volume of oscillating water (water weight =  $16 \text{ gr/in}^3$ ). With these ratios of accelerometer weight to fabric weight and water weight, the data must be affected by the accelerometer mass.

It would appear that tests of a much larger diameter (and short-length) model would be required to determine whether local oscillations of fabric, or oscillations of an entire cross section, would occur on a full-scale pipe. Based on very rough estimates of cross-section vibration-mode frequencies for a typical, full-scale pipe, significant-magnitude local or cross-section oscillations are considered unlikely. The model CWP high-frequency local oscillations occurred only when tow velocities were in excess of 0.8 ft/sec. If this velocity is Froude scaled to a full-scale pipe with a 75-foot OD, the full-scale current velocity would be 8 ft/sec. However, if this is a Reynolds number related phenomenon, the corresponding full-scale velocity could be as low as 0.008 ft/sec.

Because the high-frequency, very small amplitude oscillations were undoubtedly influenced by, or perhaps even caused by, the accelerometers, they are not expected on full-scale pipes. However, tests of a short length of large-diameter double-walled pipe would be desirable to ensure that there are no potential problems due to local or cross-section oscillations. Accelerometer weights would be less significant on a larger pipe section.

## 10. CONCLUSIONS AND RECOMMENDATIONS

### 10.1 Conclusions

- a. The annulus pressures required for cross-section stability, when the core pressure is less than the external water pressure, were greater than predicted by the classical, cylinder buckling equation.
- b. Only the first mode of vibration was well defined by the vibration tests. Natural frequencies increased as expected when the ballast weight was increased. Increases in annulus pressure also caused an increase of natural frequency.
- c. During tow tests, only the first vibration mode was excited consistently. Maximum amplitudes were less than  $\pm 1.5$  diameters. Such amplitudes would be insignificant for full-scale flexible CWP's 2000 to 3000 feet long. Amplitudes of full-scale pipes, expressed as amplitude/diameter, are expected to be less than model amplitudes because of current variation versus depth.
- d. There were indications of some local high-frequency (35 Hz) vibrations of the pipe outer wall. The amplitudes were only approximately  $\pm 0.0004$  inch. The accelerometers, although small, may have influenced or even caused these oscillations.
- e. The accelerometers were suitable instruments for measuring angular deflections in the pendulum mode. They are not suitable for measuring deflections of higher (but still very low frequency) modes because total signals are due to combinations of true accelerations and components of gravity.
- f. The model tests did not disclose any problems suggesting that the double-walled flexible pipe concept is infeasible.

### 10.2 Recommendations

- a. Existing force-balance computer programs should be modified to predict cross-section ring buckling without use of the classical, cylinder buckling equation. Revised predictions should be compared with the model data to validate the method.
- b. Tests should be conducted to measure the bending stiffness (EI) of the model. Measured EI should be compared to the calculated value.
- c. Existing computer programs should be reviewed to determine suitability for predicting model and full-scale pipe modes and frequencies, including EI and axial tension effects. If these methods are applicable, predicted modes and frequencies should be compared with the model data.

- d. The model drag deflections should be further analyzed and compared with predictions to estimate effective average Cd's, including effects of model oscillations.
- e. The vibration response curves and decaying oscillations should be further analyzed to determine damping due to external hydrodynamic damping and model internal damping coefficients.
- f. The ring buckling computer program from a., above, should be extended and used to investigate effects of alternate cross sections, including some with improved shear stiffness.
- g. Results of f. should be used with existing pipe optimization programs to define a representative design for a 30-foot-inside-diameter pipe.
- h. A selected new cross section from f. should be tested to verify buckling characteristics.
- i. Buckling characteristics should also be measured with selected annulus cells depressurized to represent failures.
- j. A higher L/D model should be designed, and lateral modes and frequencies should be determined experimentally.
- k. The beam modes and frequencies of the higher L/D model should be determined experimentally.
- l. Tests of a high L/D model should be conducted to measure core and annulus pressures, and fabric loads induced by wave passage and/or support motions.
- m. A large-diameter, short-length section should be tested in a tow tank or water current to verify that the very small amplitude, high-frequency oscillations indicated by the model tests will not be significant for full-scale pipes.
- n. Exploratory model tests with water flow in the core should be conducted to determine if any unexpected dynamic coupling between internal flow and cross-section changes could occur.
- o. Future vibration or tow tests should investigate alternatives to accelerometers for measurements of pipe dynamic motions.

REFERENCES

1. Test Plan, *Flexible Cold Water Pipe Model* (Bell Aerospace Textron, New Orleans Operations Report 2531-928001, November 9, 1978).
2. Roger King, *A Review of Vortex Shedding Research and Its Application* (Pergamon Press, Ocean Engineering, 1977) vol 4, pp 141-171.
3. Owen M. Giffin, *Vortex Shedding and the OTEC Pipe* (David Taylor Naval Ship Research and Development Center, paper presented to the Technical Workshop on OTEC at Johns Hopkins University, January 17-18, 1979).

